CHARACTERIZATION OF AUTOINFLAMMATORY MANIFESTATIOINS IN
NEMO DEFICIENCY AND ANALYSIS OF GENE EXPRESSION PATTERNS
IN LRBA AND CTLA-4 DEFICIENCIES

A THESIS SUBMITTED TO
THE GRADUATE SCHOOL OF NATURAL AND APPLIED SCIENCES
OF
MIDDLE EAST TECHNICAL UNIVERSITY

BY

NAZ SÜRÜCÜ

IN PARTIAL FULFILLMENT OF THE REQUIREMENTS
FOR
THE DEGREE OF DOCTOR OF PHILOSOPHY
IN
BIOLOGY

FEBRUARY 2022

Approval of the thesis:

CHARACTERIZATION OF AUTOINFLAMMATORY MANIFESTATIOINS IN NEMO DEFICIENCY AND ANALYSIS OF GENE EXPRESSION PATTERNS IN LRBA AND CTLA4 DEFICIENCIES

submitted by **NAZ SÜRÜCÜ** in partial fulfillment of the requirements for the degree of **Doctor of Philosophy** in **Biology, Middle East Technical University** by,

Prof. Dr. Halil Kalıpçılar
Dean, Graduate School of **Natural and Applied Sciences**   _____

Prof. Dr. Ayşe Gül Gözen
Head of the Department, **Biological Sciences**   _____

Prof. Dr. Mayda Gürsel
Supervisor, **Biological Sciences, METU**   _____

Examining Committee Members:

Prof. Dr. Safa Barış
Pediatric Immunology, Marmara University   _____

Prof. Dr. Mayda Gürsel
Biological Sciences, METU   _____

Assoc. Prof. Dr. Çağdaş Devrim Son
Biological Sciences, METU   _____

Assoc. Prof. Dr. Yasemin Özsürekçi
Pediatric Immunology, Hacettepe University   _____

Asst. Prof. Dr. Banu Bayyurt Kocabaş
Biological Sciences, METU   _____

Date: 09.02.2022

I hereby declare that all information in this document has been obtained and presented in accordance with academic rules and ethical conduct. I also declare that, as required by these rules and conduct, I have fully cited and referenced all material and results that are not original to this work.

Name Last name : Naz Sürücü

Signature :

ABSTRACT

CHARACTERIZATION OF AUTOINFLAMMATORY MANIFESTATIOINS IN NEMO DEFICIENCY AND ANALYSIS OF GENE EXPRESSION PATTERNS IN LRBA AND CTLA-4 DEFICIENCIES

Sürücü, Naz
Doctor of Philosophy, Biology
Supervisor: Prof. Dr. Mayda Gürsel

February 2022, 88 pages

NEMO (NF-κB essential modulator, IKK-γ) deficiency that phenotypically manifests as ectodermal dysplasia with immune deficiency (EDA-ID) arises due to hypomorphic mutations in the *ikbkg* gene in males. Patients present with developmental impairment of ectodermal tissues accompanied with recurrent infections early in life. Herein, we investigated the underlying mechanistic conditions leading to paradoxical autoinflammatory manifestations in a case of NEMO deficiency, who later underwent HSCT. Consistent with the immune deficiency, the patient was unable to generate pro-inflammatory cytokines IL-1β and IL-6 in response to TLR stimulation. In contrast, the patient had inflammatory low-density granulocytes (LDG) as well as primed neutrophils in the circulation that potentially induced the clinical pathophysiology. Gene expression analysis conducted with the LDG and autologous neutrophil populations from the patient revealed increased expression of adhesion and inflammation related genes, indicating their potential to cross into the tissue and inflict damage. Furthermore, the patient exhibited an elevated type I IFN signature as evidenced by high IP-10 levels in the plasma in addition to excessive ISGylation of cellular proteins. The clinical

autoinflammatory manifestations receded after HSCT parallel to the disappearance of the LDG population and the type I IFN signature, supporting their involvement in disease pathophysiology. Apart from this, we explored the gene expression profiles of CHAI and LATAIE patients, who started to receive abatacept therapy. Our preliminary data show coherence with the clinical phenotype of both disorders and display the improving effect of abatacept on the course of disease.

Keywords: Autoinflammation, CHAI, LATAIE, NEMO deficiency, low-density granulocytes (LDG)

ÖZ

NEMO EKSİKLİĞİNDE OTOENFLAMATUVAR BULGULARIN KARAKTERİZASYONU İLE LRBA VE CTLA-4 EKSİKLİKLERİNDE GEN EKSPRESYONLARININ ANALİZ EDİLMESİ

Sürücü, Naz
Doktora, Biyoloji
Tez Yöneticisi: Prof. Dr. Mayda Gürsel

Şubat 2022, 88 sayfa

Fenotipik olarak immün yetmezlikli ektodermal displazi (EDA-ID) olarak ortaya çıkan NEMO (NF-κB esansiyel modülatör, IKK-γ) eksikliği, erkeklerde *ikbkg* genindeki hipomorfik mutasyonlardan dolayı gelişir. Hastalar, yaşamın erken dönemlerinde tekrarlayan enfeksiyonlarla birlikte ektodermal dokuların gelişimsel bozukluğu ile kliniğe başvururlar. Bu çalışmada, sonradan kök hücre nakli uygulanan bir NEMO eksikliği vakasında paradoksal otoinflamatuar belirtilere sebep olabilecek mekanik koşullar araştırılmıştır. Hasta, immün eksikliği dolayısıyla beklendiği gibi TLR stimülasyonuna yanıt olarak pro-inflamatuar sitokinler IL-1β ve IL-6 üretemedi. Buna zıt olarak, hastada inflamatuar düşük yoğunluklu nötrofillerin (DYN) yanı sıra dolaşımda uyarılmış nötrofillere rastlandı. Hastadan alınan DYN ve otolog nötrofiller ile yürütülen gen ekspresyonu analizine göre, adhezyon ve enflamasyon ile ilgili genlerin ekspresyonunun artmış olması, bu hücrelerin doku hasarına sebep olma potansiyeli taşıdıkları ve böylece hastadaki klinik patofizyolojiyi kötüleştirdikleri düşünülmüştür. Ayrıca hastada, hücresel proteinlerin aşırı ISG'lasyonuna ek olarak plazmada aşırı miktarda IP-10 bulunması, hastanın dolaşımında yüksek seviyede tip I IFN imzası olduğunu göstermektedir. Nakilden sonra DYN ve tip I IFN imzasının kaybolmasına paralel olarak klinik

otoinflamatuar belirtilerin gerilemiş olması, bu bulguların hastalık patofizyolojisine katkısı olduğu şüphesini desteklemiştir. Bunların dışında, abatacept tedavisi almaya başlayan CHAI ve LATAIE hastalarının gen ekspresyon profilleri araştırılmıştır. Ön sonuçlarımız her iki bozuklukta görülen gen ifadelerinin klinik bulgular ile örtüştüğünü ve abatacept tedavisinin hastalığın seyri üzerindeki iyileştirici etkisini göstermektedir.

Anahtar Kelimeler: Otoenflamasyon, CHAI, LATAIE, NEMO eksikliği, düşük yoğunuklu nötrofiller

To my mother,

who always put education first

ACKNOWLEDGMENTS

TABLE OF CONTENTS

LIST OF TABLES

TABLES

LIST OF FIGURES

FIGURES

xviii

LIST OF ABBREVIATIONS

AIM2	Absent in melanoma 2
ALP	Alkaline phosphatase
APC	Antigen presenting cell
ASC	Apoptosis associated speck-like protein containing a CARD
BCG	Bacille Calmette-Guérrin
CARD	Caspase activation and recruitment domain
CBA	Cytometric bead array
CC	Coiled-coil
CCL	Chemokine (C-C motif) ligand
cGAS	Cyclic GMP-AMP synthase
cGAMP	Cyclic GMP-AMP
CHAI	CTLA-4 haploinsufficiency with autoimmune infiltration
CMV	Cytomegalovirus
CTLA-4	Cytotoxic T lymphocyte antigen 4
CXCL	Chemokine (C-X-C) ligand
DAMP	Danger associated molecular pattern
DAG	Diacylglycerol
DC	Dendritic cells
DHR	Dihydrorhodamine

DPBS	Dulbecco's phosphate-buffered saline
ECM	Extracellular matrix
EDA	Ectodermal dysplasia
ELISA	Enzyme linked immunosorbent assay
FACS	Fluorescence activated cell sorting
FBS	Fetal bovine serum
FSC	Forward scatter
GBP	Guanylate binding protein
GSDM	Gasdermin
HRP	Horseraadish peroxidase
HSCT	Hematopoietic stem cell transplantation
HSV	Herpes simplex virus
ICAM	Intercellular adhesion molecule
ID	Immune deficiency
IEI	Inborn errors of immunity
IFIT1	Interferon induced protein with tetratricopeptide repeat 1
IFITM	Interferon induced transmembrane
IFN	Interferon
IFNAR	IFN-α receptor
IL	Interleukin
IKK	Inhibitor of κB kinase

IP	Incontinentia pigmenti
IP-10	IFN-γ inducible protein 10
IRAK	Interleukin-1 receptor associated kinase
IRF	Interferon regulatory factor
ISG	Interferon stimulated gene
LATAIE	LRBA deficiency with autoantibodies, Treg defects, autoimmune infiltration and enteropathy
LDG	Low density granulocytes
LPS	Lipopolysaccharide
LRBA	Lipopolysaccharide-responsive and beige-like anchor protein
LSM	Lymphocyte separation medium
LZ	Leucine zipper
MAL	MyD88 adaptor-like
MAVS	Mitochondrial antiviral signaling protein
MD-2	Myeloid differentiation factor 2
MDA-5	Melanoma differentiation-associated protein 5
MDP	Muramyl dipeptide
MHC	Major histocompatibility complex
MMP	Matrix metalloprotease
MPO	Myeloperoxidase
MS	Multiple sclerosis

MyD88	Myeloid differentiation factor-88
NAIP	NLR family apoptosis inhibitory protein
NEK7	NIMA related kinase 7
NEMO	NF-κB essential modulator
NETs	Neutrophil extracellular traps
NF-κB	Nuclear factor- kappa B
NGS	Next-generation sequencing
NK	Natural killer
NLR	Nucleotide-binding oligomerization domain like receptors
NOD	Nucleotide-binding oligomerization domain
ODN	Oligodeoxynucleotide
PAMP	Pathogen-associated molecular pattern
PBMC	Peripheral blood mononuclear cells
PBS	Phosphate buffered saline
PCR	Polymerase chain reaction
pDC	Plasmacytoid dendritic cell
PGN	Peptidoglycan
PID	Primary immune deficiency
PKC	Protein kinase C
PLC	Phospholipase C
PMA	Phorbol 13-myristate 12-acetate

PMN	Polymorphonuclear
PNPP	Para-nitrophenyl pyro phosphate
PRR	Pattern recognition receptor
PYD	Pyrin domain
PYHIN	Pyrin and HIN
R848	Resiquimod
RBC	Red blood cell
RIG-I	Retinoic acid-inducible gene-I
RLR	Retinoic acid-inducible gene-I like receptor
RNA	Ribonucleic acid
ROS	Reactive oxygen species
RPMI	Roswell Park Memorial Institute
SA-AP	Streptavidin-alkaline phosphatase
SDS	Sodium dodecyl sulfate
SLE	Systemic lupus erythematosus
SSC	Side scatter
STAT	Signal transducer and activator of transcription
STING	Stimulator of interferon genes
T3SS	Type 3 secretion systems
TAK1	TGF-β activated kinase 1
TBK	TANK-binding kinase
TCR	T cell receptor

Th	Helper T-cell
TLR	Toll-like receptor
TMB	3,3',5,5'-Tetramethylbenzidine
TNF	Tumor necrosis factor
TRAF	TNF-receptor associated factor 6
TRAM	TRIF-related adaptor molecule
TRIF	TIR domain containing adaptor inducing interferon-β
ZF	Zinc finger

CHAPTER 1

INTRODUCTION

1.1   The Innate and Adaptive Immune Systems

The human body is continuously exposed to foreign molecules and infectious agents. Protection against their potential damage is provided by the immune system through the activities of effector cells and molecules. Recognition of detrimental foreign or self-originating molecular patterns by the innate immune system constitutes the immediate innate immune response. Following recognition, the immune system further recruits white blood cells, lymphocytes, and effector molecules such as the complement system in an effort to delimit and eventually eliminate infection. In case the innate system fails to achieve clearance of the damaging agent, the adaptive immune system is mobilized with specifically targeted effector T-cell and B-cells, which provide cell-mediated and humoral immunity, respectively. Adaptive immune cells harbor vast range of highly specific antigen receptors that are generated during their development. Once T-cells mature in the thymus, they circulate between the bloodstream and lymphatics as naïve T-cells until they meet their stimulatory antigen presented on the MHC (major histocompatibility complex) molecules on the surface of antigen presenting cells (APCs). $CD8^+$ cytotoxic T cells recognize antigens on MHC class I molecules, whereas $CD4^+$ helper T-cells specifically recognize peptides displayed on MHC class II molecules. T cells become activated when their antigen receptors are engaged in the presence of additional co-stimulatory signals received from the APCs. Activated T cells proliferate and then differentiate into effector cells. Helper T cell effector subclasses include T_H1, T_H2, T_H17, T_{FH} (follicular helper T-cells) as well as the inhibitory type regulatory T-cells (T_{regs}) (Murphy & Reiner, 2002). Humoral immunity, on the other hand, is provided by soluble antibodies that are able to neutralize, opsonize pathogens as well as activate the complement system.

Antibodies are generated and secreted from plasma B-cells that are activated upon antigen recognition, usually with the help of T_{FH} cells, followed by affinity maturation through genetic recombination. However, in order to keep collateral damage at a minimum level, regulation of the immune system is vital to prevent allergic or autoimmune conditions. Another fundamental function of defense against pathogens is the ability to generate immunological memory. The adaptive immune system is capable of retaining memory cells and antibodies that specifically recognize the pathogen of interest after an infection has been cleared so that a secondary exposure is met with a much stronger and more rapid response. Furthermore, recent studies provide evidence that the innate immune system is also able to establish non-specific memory functions through epigenetic modifications as well. In this functional adaptation, called trained immunity, innate immune cells such as monocytes and macrophages secrete pro-inflammatory cytokines more readily and in higher amounts in response to an unrelated secondary infection. The Bacille Calmette-Guérrin (BCG) vaccine and the fungal cell wall element β-glucan have been demonstrated to exert this type of innate immune memory (Arts et al., 2018).

1.1.1   The Innate Immune System

Mucosal surfaces and antimicrobial proteins act as physical and chemical barriers against pathogenic agents. In case these barriers are breached, the first responders that are sent by the host are components of the innate immune system. While antimicrobial enzymes and peptides can digest and lyse bacterial surfaces, the complement system is able to target pathogens for lysis and phagocytosis in a series of proteolytic cleavage reactions involving soluble plasma proteins. In parallel, recruitment of innate immune cells from the local tissue as well as from the circulation to the site of inflammation is achieved through the secretion of chemokines and cytokines from sensor cells in the tissue. Monocytes from the circulation continuously localize into the tissue and differentiate into phagocytic tissue-resident macrophages, that are able to engulf and eliminate tissue invading

pathogens and infected cells (Janeway & Medzhitov, 2003). Another critical role of macrophages in the advancement of inflammation is to secrete inflammatory mediators in order to recruit and activate other immune cells. Dendritic cells (DC) are an additional class of phagocytes, that can sample large amounts of extracellular fluid in a process known as macropinocytosis and degrade engulfed microorganisms. Importantly, DC are capable of migrating to the nearest lymph node and activate T-cells of the adaptive immune system through antigen presentation on MHC molecules. Furthermore, like macrophages, DC also release mediators for immune cell recruitment and activation. The third class of phagocytic cells of the innate immune system are the granulocytes, comprised of neutrophils, mast cells, eosinophils and basophils. Altogether, innate immune cells comprise the first line of defense against tissue invading pathogens through their rapid and invariant recognition.

1.1.1.1   Innate Immune Detection and Pattern Recognition Receptors (PRRs)

Macrophages, dendritic cells, and neutrophils are vital effectors of the innate immune response. Their activation through the stimulation of either cell surface or cytosolic receptors instigates tissue inflammation required for pathogen clearance (Beutler & Rietschel, 2003). Innate immune activation is distinct from an adaptive immune response in the sense that it arises in a few hours post-infection. This rapid response is ensured by a series of sensors, collectively known as pattern recognition receptors (PRRs), which are specific to evolutionarily conserved patterns on microorganisms known as pathogen associated molecular patterns (PAMPs) (Aderem & Underhill, 2003). Moreover, it was later shown that these receptors are also able to detect host derived molecules called danger associated molecular patterns (DAMPs) released from injured or dying cells. Extracellular PAMPs are detected through toll-like receptors (TLRs) that are found on the plasma membrane and membranes of endosomal vesicles (Kawai & Akira, 2007). TLRs are categorized

depending on their activating ligands. For instance, the heterodimers TLR1 and TLR2 as well as TLR2 and TLR6 on the cell membrane, are able to sense lipoproteins originating from Gram-negative bacteria (Jin et al., 2007). TLR4, another cell membrane bound receptor, together with the accessory protein MD-2 detect the lipopolysaccharide (LPS) of Gram-negative bacteria (Park et al., 2009). TLR5, also residing on the plasma membrane, recognizes a globular protein in the bacterial flagellum known as flagellin. Endosomal TLRs, on the other hand, are specialized in the detection of nucleic acids. Of those, TLR3 is able to recognize dsRNAs of viruses or infected dying cells (L. Liu et al., 2008). Other endosomal receptors such as TLR7 and TLR8, have evolved to sense ssRNA molecules, rendering them indispensable against immunity to ssRNA viruses (Heil et al., 2004). TLR9, however, can detect unmethylated CpG motifs that are distinctly found at higher frequency in bacterial and in some viral genomes (Lund, Sato, Akira, Medzhitov, & Iwasaki, 2003). The activation of TLRs leads to their dimerization that brings their cytoplasmic TIR domains into close proximity, inducing the recruitment of adapter molecules MyD88, MAL, TRIF, or TRAM (Werts, Girardin, & Philpott, 2006). Different TLRs utilize alternative combinations of adapter molecules, of which MyD88 is the most prominent adaptor involved in downstream TLR signaling. MyD88, facilitates the recruitment of the serine-threonine kinases IRAK1 and IRAK4, which attract the E3 ubiquitin ligase TRAF6 (Werts et al., 2006). This enzyme enables the construction of a scaffold for the recruitment of the serine-threonine kinase TAK1 through the formation of K63 polyubiquitin chains. Next, TAK1 phosphorylates the IκB kinase (IKK) complex, which comes into close proximity through interactions of the IKK regulatory subunit NEMO (IKK-γ) to the polyubiquitin chains. Then, the activated IKK complex, phosphorylates the cytosolic inhibitor of κB (IκB) that is bound to the transcription factor NF-κB, composed of the subunits p50 and p65. Upon its release, NF-κB translocates into the nucleus, where it induces transcription of genes encoding the pro-inflammatory cytokines TNF-α, IL-1β and IL-6. On the other hand, antiviral sensing by endosomal TLRs induces the phosphorylation and subsequent translocation of IRF (interferon

regulatory factor) family transcription factors (Honda & Taniguchi, 2006). Of those, especially IRF3 and IRF7 are crucial mediators in the induction antiviral type I interferon production (Kawai et al., 2004).
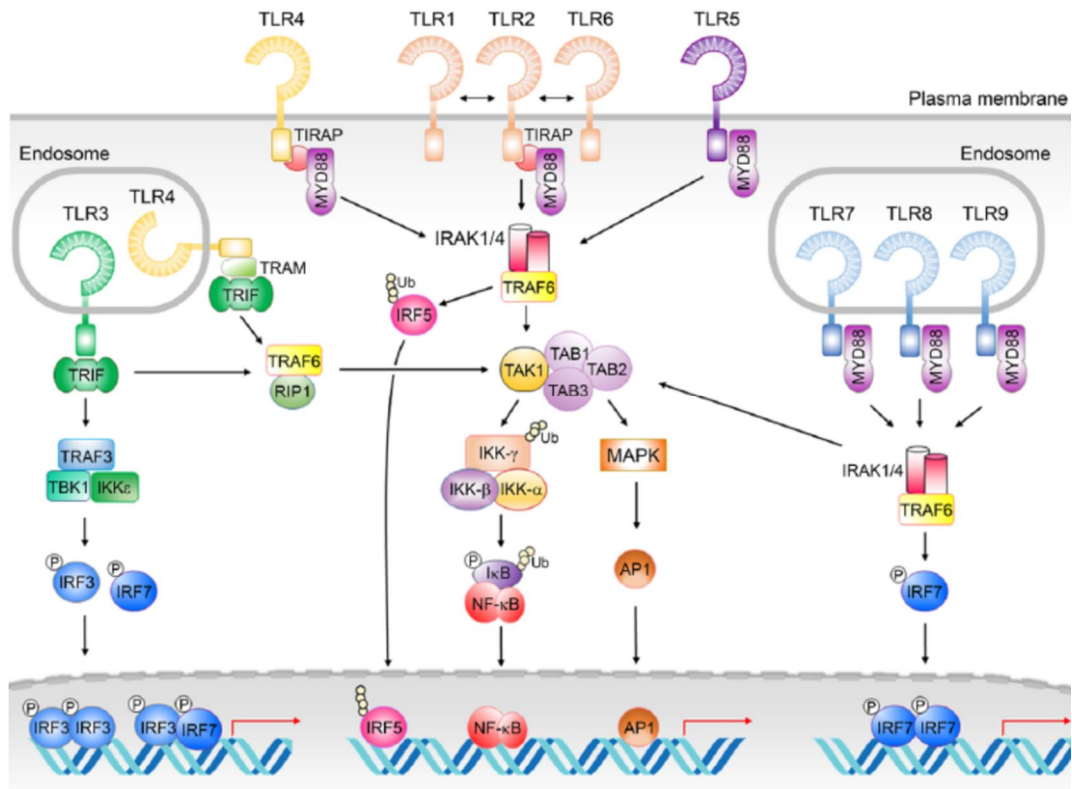
Figure 1.1 : Illustration of TLR signaling. Adapted from (Chen, Shih, Hung, and Hsueh, 2019)

While TLRs are sensors for the extracellular environment, intracellular surveillance is partially ensured by another family of PRRs known as NOD-like receptors (NLRs) (Werts et al., 2006). NLRs are also able to induce NF-κB activation as well as pro-inflammatory cytokine secretion through another cell death involved pathway (Shaw, Reimer, Kim, & Nuñez, 2008). The NOD proteins are specialized to recognize breakdown components of peptidoglycan (PGN), originating from bacterial cell walls. The NOD1 protein senses γ-glutamyl diaminopimelic acid (iE-DAP), whereas NOD2 is able to detect muramyl dipeptide (MDP) (Strober, Murray,

Kitani, & Watanabe, 2006). Another group of NLRs, which are called NLRP due to their pyrin domains, oligomerize upon activation, forming a multiprotein structure known as the inflammasome. Depending on the stimulatory agent, different types of inflammasomes can be formed that were identified as NLRP1, NLPR3, NLPR6, NLPR7, NLRP12, NLRC4, and AIM2 (Kofoed & Vance, 2011). Downstream events proceed with the oligomerization of ASC (apoptosis associated speck-like protein containing a caspase recruitment domain) forming a scaffold to recruit pro-caspase1, which undergoes proximity induced proteolytic cleavage (Hornung et al., 2009). Next, the outcome of inflammasome activation converge on the proteolytic cleavage of pro-inflammatory cytokine precursors such as pro-IL-1β and pro-IL-18 by caspase-1 (Hornung et al., 2009). Following cleavage, active forms of these cytokines are released through pores that are formed on the plasma membrane through the activity of gasdermin D (GSDM-D), leading to a pyrogenic form of cell death known as pyroptosis.

Another intracellular receptor family, identified as RIG-I-like receptors (RLRs) are able to sense intracellular pathogen derived RNA motifs. One member of this receptor family known as RIG-I (retinoic acid inducible gene I) was discovered to recognize ssRNA molecules lacking the 5'triphosphate 7-methyguanosine cap that is exclusive to eukaryotic RNA synthesized in the nucleus (Hornung et al., 2006). Additionally, the MDA-5 (melanoma differentiation-associated 5) receptor was found to detect dsRNA in the cytosol. The activation of either RIG-I or MDA-5 leads to their interaction with the adapter molecule MAVS (mitochondrial antiviral signaling protein) through a K63 polyubiquitin platform similar to TLR signaling (Kato et al., 2006). MAVS recruitment results in further K63 ubiquitination events which enable the attraction of TBK1 (TANK-binding kinase 1) and IRF3, followed by the induction of type I IFN production in parallel to NF-κB activation (Pichlmair et al., 2006).
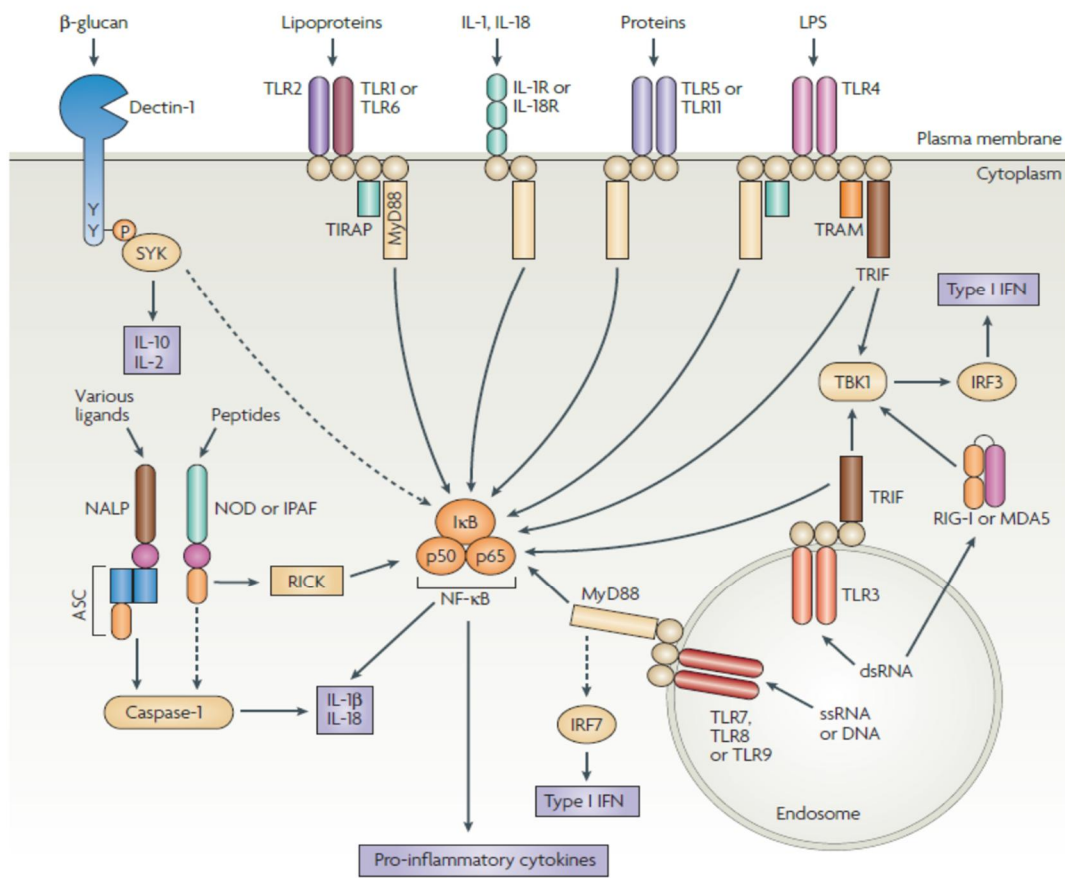
Figure 1.2 Illustrations of PRR signaling. Adapted from (Trinchieri and Sher, 2007)

Intracellular DNA detection takes place through the activity of the cGAS (cyclic GMP-AMP synthase) enzyme, that upon activation starts the production of a secondary messenger identified as cGAMP (cyclic GMP-AMP) (Cai, Chiu, & Chen, 2014). This molecule, then binds to the ER resident STING (stimulator of interferon genes) homodimer, changing its conformation, which in turn enables the activation of TBK1 and downstream phosphorylation of IRF3 (Ishikawa & Barber, 2008) (Tanaka & Chen, 2012). Parallel to MAVS signaling, IRF3 then translocates to the nucleus to initiate type I IFN production (S. Liu et al., 2015).

Interferons are essential constituents of the host defense against viral infections due to their ability to interfere with viral replication. These cytokines are classified into three groups as type I (IFN-α, IFN-β), type II (IFN-γ), and type III (IFN-λ, IL-28A,

IL-28B, IL-29) interferons, of which type I IFNs are the most studied group (Honda, Takaoka, & Taniguchi, 2006) (Pott et al., 2011). The induction of type I IFN production through the activation of either TLR3/TLR7/TLR9, RIG-I/MDA5, or the cGAS-STING pathways results in the stimulation of IFNAR (interferon-α receptor) (Honda et al., 2006). Downstream signaling initiates the activation of the Jak-STAT (signal transducer and activator of transcription) pathway, leading to the recruitment of STAT1 and STAT2, which are then able to interact with IRF9, forming the ISGF3 complex, eventually driving the expression of interferon stimulated genes (ISGs) (Levy & Darnell, 2002).
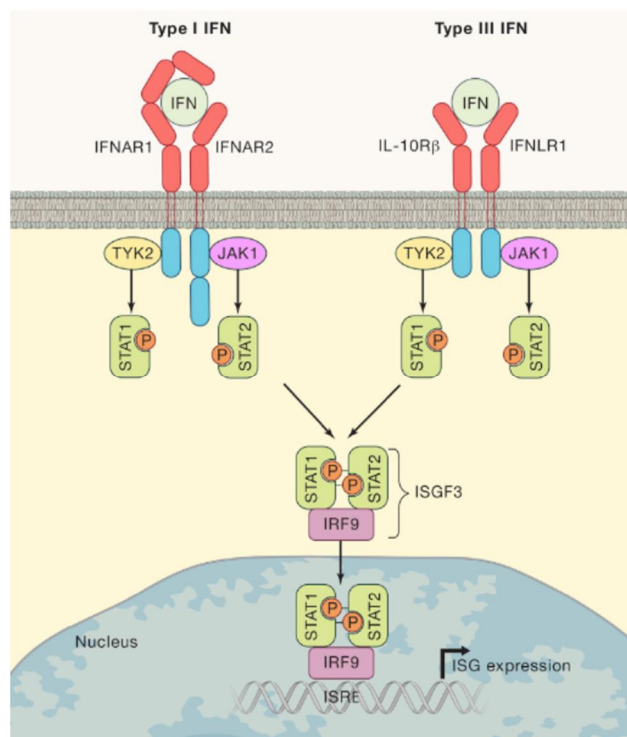
Figure 1.3 Illustration of type I and type III IFN signaling. Adapted from (Lazaer, Schoggins, and Diamond, 2019)

The induction of ISGs such as Mx1, IFIT1, and IFITM enables interference with viral propagation (Malterer, Glass, & Newman, 2014). This is partially achieved

through the inhibition of translational processes such as hindering the formation of ribosomal translation complexes. Furthermore, interferon induced proteins are able to disturb the fusion of viral membranes with lysosomes, obstructing their access to the cellular translational machinery (Malterer et al., 2014). Importantly, ISGs are also able to increase the production of certain chemokines such as CXCL9, CXCL10 (IP-10), and CXCL11 (M. Liu et al., 2011). Chemokine secretion facilitates further recruitment of immune cells towards the site of infection. Moreover, ISG products enhance MHC class I expression on host cells, accelerating the recognition of virus infected cells by cytotoxic T-cells of the adaptive immune system. Another significant member of ISGs was discovered to be ISG15. Studies conducted in the past decade provide evidence that ISG15 has the ability to modify various protein functions (Perng & Lenschow, 2018). It does so through ubiquitin-like post-translational covalent conjugation to cellular proteins in a process called ISGylation upon type I IFN signaling (Loeb & Haas, 1992). While its exact mechanism of action remains to be elucidated, previous research demonstrates that free ISG15 can also act in an antiviral manner either intracellularly or as an extracellular cytokine (Perng & Lenschow, 2018). Together, the aforementioned innate immune mechanisms constitute a fundamental front against invading pathogens as the first line of host defense.

1.1.1.2   Polymorphonuclear (PMN) Leukocytes

Neutrophils, also known as polymorphonuclear leukocytes, are short-lived and the first phagocytic cells to be recruited in large numbers to the site of inflammation (Rosales, 2018). Once a microorganism is recognized as potentially dangerous by resident macrophages, they start the secretion of lipid mediators such as prostaglandins and leukotrienes as well as chemokines and cytokines for the establishment of inflammation in the infected tissue. The release of inflammatory mediators triggers vasodilation of nearest blood vessels, thereby easing the passage of monocytes and neutrophils into the tissue. Through the interaction with P and E

selectins on endothelial surfaces, neutrophils start to slow down and roll along the endothelial lining until a strong enough connection is formed with the adhesion molecules ICAM-1 and ICAM-2 to cease movement of the cells (Adrover et al., 2019). Next, ECM degrading enzymes facilitate the extravasation of neutrophils between endothelial cells towards the cytokine and chemokine gradient created by macrophages in the tissue (Kolaczkowska & Kubes, 2013). Upon entry, neutrophils are able to utilize three separate mechanisms for pathogen clearance. As neutrophils are proficient phagocytes, one way of pathogen removal is through the engagement of their surface receptors to either PAMPs or to the Fc portions of immune complexes formed on the microorganism. This receptor-mediated uptake leads to the formation of a phagolysosome through the fusion of the phagocytic vacuole with intracellular granules containing degrading enzymes acting at low pH conditions. Another mechanism for pathogen neutralization by neutrophils is the fusion of proteinase and antimicrobial peptide containing primary and secondary granules with the plasma membrane as well as their leakage during phagosome formation (Borregaard & Cowland, 1997). These granules are dominantly comprised of cathelicidins and α-defensins which can act on negatively charged membrane structures by inducing pore formation and membrane permeabilization. Moreover, secreted antimicrobial peptides are able to attract immune cells and stimulate cytokine secretion, thereby promoting host defense and tissue inflammation (Chertov, Yang, Zack Howard, & Oppenheim, 2000). Alternatively, neutrophils can utilize a distinct form of cell death involving the formation of neutrophil extracellular traps (NETs) through the condensation of chromatin and its decoration with antimicrobial granular proteins and enzymes such as neutrophil elastase and myeloperoxidase (MPO) (Brinkmann & Zychlinsky, 2007). The proteins that decorate NET structures, like LL-37, S100A, and lactoferrin have microbicidal properties that act on pathogens upon their entrapment.
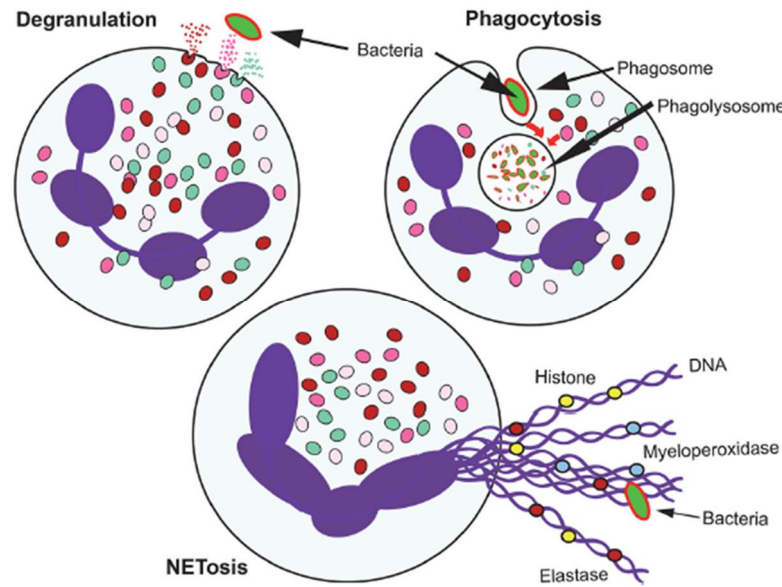
Figure 1.4 Illustration of killing mechanisms employed by neutrophils. Adapted from (Rosales, 2018)

Neutrophil-mediated pathogen clearance requires the production of reactive oxygen species (ROS) through the activity of the transmembrane enzyme NADPH-oxidase, which is activated through the co-localization with components found on the membrane such as gp22^{phox}, gp91^{phox} (NOX2) and p40^{phox}, p47^{phox}, and p67^{phox} found in the cytosol (Bogdan, Röllinghoff, & Diefenbach, 2000) (Dahlgren & Karlsson, 1999). While killing mechanisms employed by neutrophils are vital for pathogen elimination, they can become extremely damaging in cases of sterile autoinflammation (Hidalgo, Chilvers, Summers, & Koenderman, 2019). Poor control of neutrophil activation by autoantibodies, immune complexes, or inflammatory cytokines can lead to extensive tissue damage through the redundant release of ROS products and granule-derived antimicrobial proteins (Hidalgo et al., 2019).

1.1.1.3 Low-Density Granulocytes (LDGs)

Earlier studies exploring the pathogenesis of autoinflammatory disorders such as systemic lupus erythematosus (SLE) and rheumatoid arthritis, report the detection of low buoyant neutrophils in the blood of patients (Hacbarth & Kajdacsy☐Balla, 1986). Further investigations revealed that these cells carry signatures of granulopoiesis, suggesting that they are immature granulocytes which are released prematurely from the bone marrow (Bennett et al., 2003). More recent studies conducted with SLE patients demonstrate that LDGs have an increased capacity of inducing vascular tissue damage while displaying decreased competence in phagocytic activity (Denny et al., 2010). The cytotoxic ability of LDGs is attributed to their enhanced production and secretion of inflammatory cytokines TNF-α and IFN-α. In short, LDGs are characterized as a distinct inflammatory cell population that carry the potential of inducing accelerated pathogenesis. Furthermore, LDGs inflict vascular damage through their increased propensity to mobilize NETosis.

1.2 Human Inborn Errors of Immunity (IEI)

Primary immune deficiencies (PIDs) arise due to mutations affecting the development or function of the immune system. Decades of ongoing research on the pathogenesis of immune deficiencies, autoinflammation, allergies, or malignancy that result from monogenic defects in innate or adaptive immunity, has identified 431 inborn errors of immunity up to date (Notarangelo, Bacchetta, Casanova, & Su, 2020). Advances in the field of therapeutic interventions such as hematopoietic stem cell transplantation (HSCT) has increased the quality of life and survival expectancy of patients significantly.

1.2.1   NEMO deficiency

As reviewed earlier, NEMO (IKK-γ) is the regulatory subunit of the IKK complex responsible for the phosphorylation of IκB and subsequent release of the transcription factor NF-κB (Michael Karin, 1999). It has fundamental functions in the activation of innate and adaptive immune responses. PRR downstream signaling cascades depend on the recruitment of the IKK complex for which the NEMO subunit interacts with polyubiquitination sites, bringing the complex into close proximity as well as stabilizing the interface. Furthermore, the IKK complex takes part also in the downstream signaling of the TNF receptor superfamily, including CD40, as well as IL1R and IL-18R in the context of furthering innate immune stimulation (M. Karin & Delhase, 2000). On the other hand, NEMO protein has vital roles in the induction of adaptive immunity as well. T-cell receptor (TCR) activation results in the generation of diacylglycerol (DAG) through phospholipase C (PLC-γ) recruitment and activation on the cell membrane (Gudmundsdottir, Wells, & Turka, 1999). This leads to the activation of three distinct downstream events, one of which comprises the recruitment of protein kinas C (PKC-θ), which in turn phosphorylates the molecule CARMA1 that acts as a scaffold for the E3 ubiquitin ligase TRAF6. Next, TAK1 interacts with the polyubiquitin chain to subsequently phosphorylate the IKK complex. The IKK activation leads to the release of the transcription factor NF-κB and the production of T-cell specific genes for the cytokines IL-2 and IFN-γ. Furthermore, B-cell activation for the generation of antibody subclasses through isotype switching recombination requires the stimulation of CD40 by CD40 ligand (CD40L) expressed on T-cells. This interaction triggers a signaling pathway through the IKK complex eventually activating NF-κB, leading to class switching and germinal center formation.
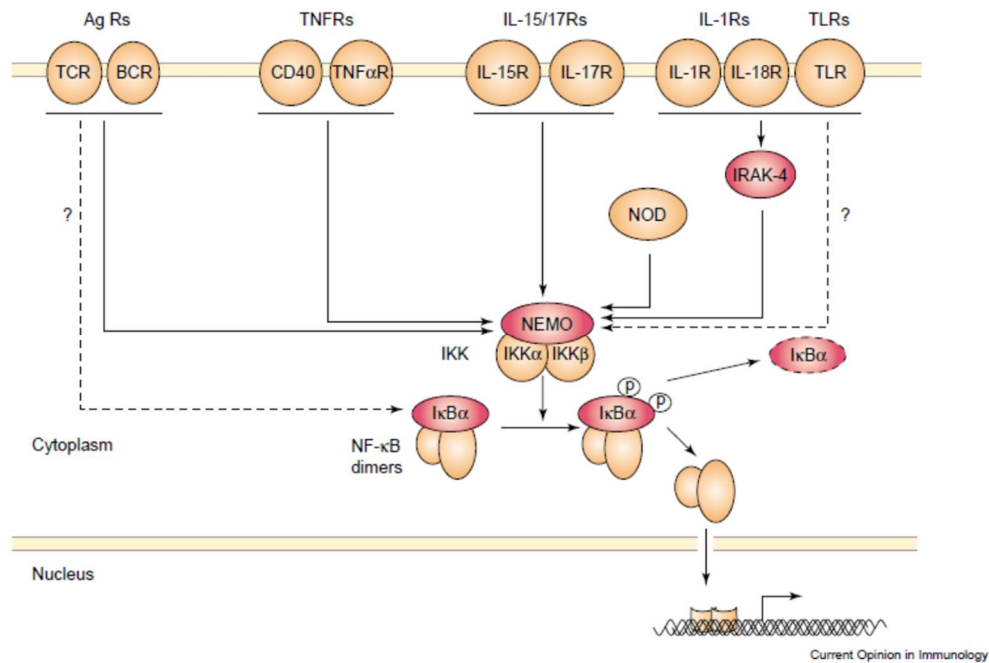
Figure 1.5 Illustration of the functional role of NEMO in downstream receptor signaling pathways. Adapted from (Puel, Picar, Ku, Smahi, and Casanova, 2004)

While the complete absence of NEMO in males is embryonically lethal, females develop incontinentia pigmenti (IP). On the other hand, hypomorphic mutations in the X-linked *ikbkg* gene in males, results in ectodermal dysplasia with immunodeficiency (EDA-ID), which manifests as developmental impairments in ectodermal tissues usually accompanied with immune deficiency (Ramírez-Alejo et al., 2015). Patients with EDA-ID, depending on its expressivity, may exhibit conical shaped partial or complete absence of teeth, sparse hair and eyebrows, and hypohidrosis. The heterogeneity in severity has been associated with the structural alterations in the NEMO protein as a consequence of various mutations. Life expectancy of EDA-ID has been associated with the severity of the immune deficiency seen in patients. While affected children may experience multiple severe bacterial infections in early infancy, EDA cases without immune deficiency have been documented as well. The most frequent infections observed in EDA-ID patients are by pyogenic bacteria such as *S.aureus*, *S.pneumoniae*, *H.influenzae*, possibly

14

explained by the lack of polysaccharide specific antibodies in these patients, and also the intracellular pathogen *Mycobacterium avium* (Fusco et al., 2015). Infections of fungal or viral origin by *Cytomegalovirus* (CMV) have been reported as well. Mutations resulting in more severe cases can also lead to osteopetrosis and lymphedema (OL-EDA-ID), an abnormal increase in bone density and fluid accumulation in soft tissues, respectively. Patients generally exhibit an impaired response to immunological mediators such as IL-1β, IL-18, TNF-α, LPS, and CD40L due to the aforementioned downstream role of NEMO in their signaling cascades, partially also contributing to the occurrence of recurrent infections.

1.2.2   CTLA-4 and LRBA deficiencies

Effector T-cells of the adaptive immune system require two stimulatory signals for activation, one of which is provided by the engagement of the T-cell receptor (TCR) to the MHC (major histocompatibility complex) molecule on specialized antigen presenting cells (APCs) (Sharpe, 2009). The second is defined as the co-stimulatory signal and involves the interaction of B7 and TNF family members such as CD28 (B7), CD27, OX40, CD137 (4-1BB) and CD40L on T-cells with their corresponding ligands on APCs (Acuto & Michel, 2003). The best studied of all is the CD28 receptor which binds to the B7.1 (CD80) and B7.2 (CD86) surface ligands on APCs (Frauwirth et al., 2002). However, the cytotoxic T lymphocyte antigen 4 (CTLA-4) is able to bind B7 with higher affinity and avidity than CD28 and induce an inhibitory signal to halt T-cell proliferation, the mechanism of which is still not fully elucidated (Rudd, Taylor, & Schneider, 2009). The importance of CTLA-4 signaling lies in the balance of allowing efficient T-cell activation while simultaneously maintaining tissue integrity by prevention of autoimmunity. Regulatory helper T-cells (T_{regs}) constitutively express CTLA-4, whereas naïve T-cells express low levels of CTLA-4 in intracellular membrane compartments (Chen & Flies, 2013). Upon activation, CTLA-4 is shuttled to the plasma membrane, where it competes with CD28 for B7 ligands (Rudd et al., 2009). Of note, CTLA-4 has been targeted for checkpoint

blockade therapy in cancer immunotherapy studies in order to increase T-cell mediated anti-tumor activity (Hodi et al., 2010). Loss-of-function mutations in CTLA-4 leading to its partial absence have been documented in humans in the last decade. Patients with CHAI (CTLA-4 haploinsufficiency with autoimmune infiltration) expectedly exhibit lymphoproliferation as well as lymphocytic infiltration of non-lymphoid organs such as the gut, lungs, and brain (Lo et al., 2016). Another symptom of CHAI includes hypogammaglobulinemia, partially accounting for the recurrent infections experienced by the patients (Lo et al., 2016). Additionally, lymphadenopathy and autoantibody mediated autoimmune cytopenia is also observed in CHAI patients (Lo et al., 2016).

Another primary immune deficiency initially known as LRBA deficiency and later called LATAEI (LRBA deficiency with autoantibodies, Treg defects, autoimmune infiltration, and enteropathy) converges with CTLA-4 deficiency in terms of clinical manifestations as both disorders result in diminished CTLA-4 presence on the plasma membrane (Gámez-Díaz et al., 2016). Initial investigations on the function of the approximately 319kDa LRBA protein suggested a role in intracellular vesicle trafficking, including CTLA-4 containing vesicles (Wang, Howson, Haller, & Kerr, 2001). Further studies narrowed the relation of how LRBA regulates CTLA-4 shuttling in T-cells to an interaction with the cytoplasmic tail of CTLA-4, thereby preventing its contact with the clathrin-associated adaptor protein complex AP-1 which guides CTLA-4 for lysosomal degradation (Lo et al., 2015).
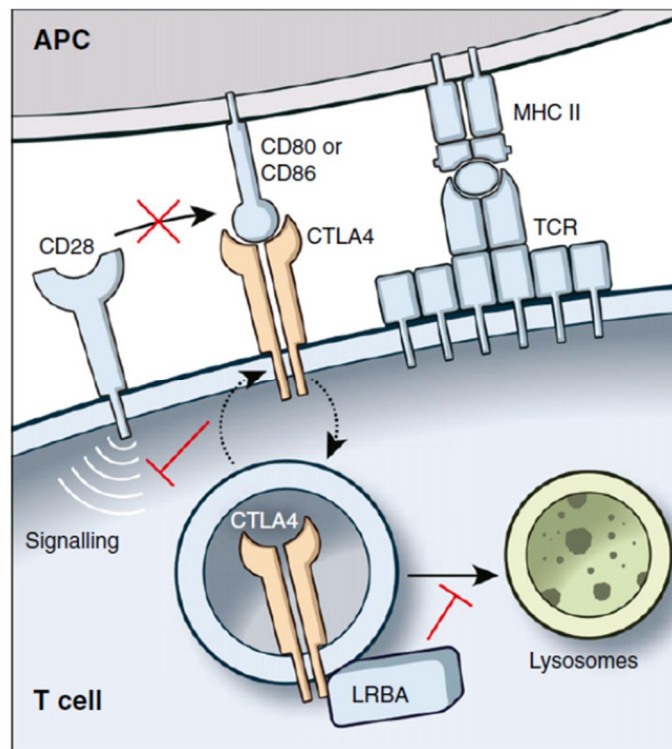
Figure 1.6 Illustration of the roles of CTLA-4 and LRBA in T-cell immunity. Adapted from (Lo et al., 2016)

Similar to CHAI, LATEI patients also display lymphocytic overactivation causing tissue infiltrations, hypogammaglobulinemia, lymphadenopathy and autoimmune cytopenia (Lo et al., 2016). Despite major similarities, the course of the disease can show certain variations in clinical phenotype as well. Due to the biallelic nature of mutations leading to LATAEI development, usually disease onset occurs at an earlier stage in life. Furthermore, the overall functions of the LRBA protein have not yet been fully elucidated, so its unknown potential roles in cellular pathways may partially account for the variation in LATAEI symptoms. Clinical studies provide evidence that treatment with abatacept, a CTLA-4-Ig fusion protein, greatly improves physical health and life quality of LATAEI and CHAI patients (Lo et al., 2015).

1.3   Aim of the Study

The molecular structure and function of the NEMO protein as the regulatory subunit of the IKK complex has been extensively studied. Furthermore, numerous cases of NEMO deficiency have been documented in which the most common phenotype is reported as ectodermal dysplasia with immune deficiency (EDA-ID). Disease onset generally arises in early childhood with recurrent infections. Additionally, affected children display impairment in the development of ectodermal tissues that manifest as hypohidrosis, conical teeth, sparse hair and eyebrows with immune deficiency. However, rare occurrences of autoinflammation in NEMO deficiency and their underlying causes have not been fully understood. In this study, we aimed to investigate the mechanistic events leading to painful nodular skin lesions, subcutaneous swelling, perivascular and interstitial neutrophilic infiltrations. In this context, we first tried to verify the NEMO deficiency with immunoblotting and explored its functional extent by stimulating freshly isolated PBMC from the patient as well as healthy controls and measured pro-inflammatory cytokine secretion. In order to determine potential circulating inflammatory cell groups, we characterized the constituents of the PBMC cell populations from the patient and healthy individuals through cell type specific surface marker labeling and subsequent flow cytometry analysis. Furthermore, we utilized the membrane-permeable initially non-fluorescent ROS indicator dihydrorhodamine123 (DHR123), that emits green fluorescence upon oxidation to compare NEMO deficient and healthy neutrophil activation states. To explore the involvement of type I IFN in the pathophysiology of the patient, we performed cytometric bead array (CBA) and ELISA to measure IP-10 levels in the patient plasma. Additionally, we used immunoblotting to detect the degree of ISGylation of cellular proteins as a consequence of type I IFN signaling. To understand the autoinflammatory state at the gene expression level we utilized the Inflammation and PanCancer Immune Profiling gene expression panels. Aside from this part of the study, we also tried to grasp the gene expression profiles of CHAI and LATAIE patients, to determine potential target pathways for further

functional analysis and the effect of abatacept treatment. In this context, we utilized the Host Response gene expression panel and compared gene expression levels of patient PBMC from different time points to healthy expression.

CHAPTER 2

MATERIALS AND METHODS

The materials and methods employed in this study are listed and described in the following sections.

2.1   Materials

2.1.1   Patient and healthy donor blood samples

This study was approved by the Ethics Committee of Marmara University, School of Medicine. Written informed consent was obtained from the patient and parents. Blood samples were drawn at Marmara University Pendik Teaching and Research Hospital Department of Pediatric Allergy and Immunology.

2.1.2   Reagents

The reagents that were used during PBMC and neutrophil isolation protocols from whole blood samples are listed in Table 2.1.

Table 2.1 Reagents used for primary cell extraction from whole blood.

Name	Company	Catalog #
DPBS (Dulbecco's phosphate-buffered saline)	Biological Industries (BI)	(BI02-023-1A)
Lymphocyte Separation Media	Capricorn	LSM-A

Table 2.1 (cont'd) Reagents used for primary cell extraction from whole blood.

Name	Company	Catalog #
RPMI1640	Biological Industries (BI)	(BI01-100-1A)
Dextran from *Leuconostoc mesenteroides*	Sigma-Aldrich	D4876-50G

Isolated PBMC and neutrophils were washed and cultured in 2% and 10% FBS supplemented RPMI1640, respectively (Appendix A). Treatments were carried out in sterile 96-well flat bottom tissue culture plates (Sarstedt, #83.3924). Identity of stimulants/PRR agonists and their working concentrations used in PBMC or neutrophil stimulation experiments are given in Table 2.2

Table 2.2 List of PRR agonists/stimulants used in stimulation experiments.

Name	Pathway	Company & Catalog #	Working concentration
PMA (phorbol 12-myristate 13-acetate)	PKC	Invivogen tlrl-pma	50 ng/ml
ionomycin	DAG	Invivogen inh-ion	1 μg/ml
LPS (lipopolysaccharide) from *Escherichia coli*	TLR4	Sigma-Aldrich L2630	1 μg/ml
R848 (resiquimod)	TRL7/8	Invivogen tlrl-r848	5 μg/ml
zymosan	TLR2	Invivogen	10 μg/ml

Table 2.2 (cont'd) List of PRR agonists/stimulants used in stimulation experiments.

Name	Pathway	Company & Catalog #	Working concentration
PAM3CSK4	TLR1/2	Invivogen tlrl-pms	1 µg/ml
flagellin	TLR5	Invivogen tlrl-epstfla	1 µg/ml
HSV60	cGAS	Invivogen tlrl-hsv60n	5 µg/ml
IFN-β (interferon-β)	IFNAR1/2 – JaK/STAT	Merck - Serono	100 ng/ml

Trizol™ Reagent (Thermo Fisher Scientific, #15596026) was used for RNA extraction as described in section 2.2.8. Chloroform (#102431) and isopropanol (#101040) were both purchased from Merck. RNA Clean & Concentrator (Zymo Research, #R1018) kit was alternatively used for RNA isolation. NanoString nCounter Inflammation (#XT-CSO-HIN2-12), Human PanCancer Immune Profiling (#XT-CSO-HIP1-12), Human Host Response (#XT-HHR-12) gene expression panels were utilized as detailed in 2.2.9.

2.1.3   Antibodies and Kits

The antibodies used for low-density granulocyte (LDG) surface staining experiments are described in Table 2.3

Table 2.3 Antibodies against cell surface markers.

Name	Company & Catalog #	Working concentration
anti CD14- PE	BioLegend #325606	3µl/test
anti-CD15- FITC	BioLegend #301904	5µl/test

Table 2.3 (cont'd) Antibodies against cell surface markers.

Name	Company & Catalog #	Working concentration
anti-CD66b-PerCP/Cy5.5	BioLegend #305108	5µl/test

Dihydrorhodamine (DHR) 123 was used for reactive oxygen species (ROS) detection in neutrophils and purchased from Thermo Fisher Scientific (#D23806). Antibodies that were utilized for immunoblotting and ELISA kits for cytokine detection are listed in Table 2.4.

Table 2.4 Western blot antibodies and ELISA kits.

Type	Name	Company	Catalog #
Western antibodies	anti-ISG15	Santa Cruz Biotechnology	sc-166755
	anti-NEMO (IKK-γ)	BioLegend	694102
		abcam	244244
		Santa Cruz Biotechnology	sc-166398
	anti-GAPDH	Santa Cruz Biotechnology	
	anti-mouse IgG, HRP	Cell Signaling Technology	7076
	anti-rabbit IgG, HRP	Cell Signaling Technology	7074
	anti-rat IgG	BioLegend	405405
ELISA kits	IFN-γ	MABTECH	3420-1A-20
	Purified IL-6	BioLegend	501102
	Biotin IL-6	BioLegend	501202
	IL-1β	MABTECH	3416-1A-20
	CXCL10	BD Biosciences	558280
	(IP-10)	BioLegend	439904

2.2 Methods

2.2.1 PBMC and Polymorphonuclear (PMN) Phagocyte Isolation

Whole blood from the patient, the mother, the father, and healthy control donors were taken into 50ml sterile collection tubes and mixed at a 1:1 volume ratio with DPBS. Next, 15ml collection tubes were layered with lymphocyte separation medium (LSM) at the bottom and 1:1 diluted whole blood at the top according to a 1:1.5 ratio. The collection tubes were centrifuged at 1800rpm for 30 minutes at room temperature with the break off to enable the formation of clear distinct layers in the order of plasma at the top, white and cloudy PBMC coat over the remaining LSM layer, and granulocytes over a bulk of red blood cells (RBCs) at the bottom. The PBMC layers from each donor were collected with plastic Pasteur pipettes into separate sterile 50ml plastic tubes and washed twice with wash media (RPMI 1640 supplemented with 2% FBS) by centrifugation at 1800rpm for 10 minutes at room temperature. Next, the PBMC were resuspended in culture media (RPMI 1640 supplemented with 10% FBS) and counted with a flow cytometer (Novocyte 2060, Agilent Technologies).

For PMN isolation, following the removal of the plasma and PBMC layers, the leftover LSM was aspirated until only the granulocyte and RBC populations remained. Subsequently, the remaining volume was completed with DPBS to the initial whole blood volume that was layered in the 15ml tube and mixed thoroughly. Then, 3% (w/v) dextran in DPBS was added onto the suspension at a 1:1 ratio. The tubes were inverted strictly 10 times and left upright at room temperature for 20 minutes to allow the gravitational separation of two layers, the top containing PMNs while the bottom layer was rich in RBCs. PMNs were collected with a plastic Pasteur pipette into another sterile 50ml collection tube to be washed with DPBS by centrifugation at 300g for 10 minutes at room temperature. After aspiration, the pellet was incubated in ACK (Ammonium-Chloride-Potassium) lysis buffer for 2-3 minutes at room temperature to lyse the residual RBC population. The ACK buffer

was then diluted with cold DPBS and the cells were pelleted for another washing step with cold DPBS at 300g and 4°C for 10 minutes. The neutrophil rich granulocyte population was resuspended in culture medium and counted using a flow cytometer (Novocyte, Agilent Technologies).

2.2.2   Low-Density Granulocyte (LDG) Staining from PBMC

At least 500,000 PBMC were resuspended in 100μl of FACS buffer (Appendix A) containing fluorochrome conjugated anti-CD14, anti-CD15, and anti-CD66b antibodies and incubated on ice for 30 minutes. Next, the antibody cocktail was diluted with 1ml of FACS buffer followed by centrifugation at 300g and 4°C for 10 minutes as a washing step. The samples were then washed once more as described and resuspended in 300μl of FACS buffer for flow cytometric analysis. As LDG are of granulocytic origin, therefore larger and more granular than other cell populations, gating was done on the population at the highest FSC-SSC scale. LDG were further identified based on their $CD14^{dim}CD15^{hi}$, $CD14^{dim}CD66b^{hi}$, and $CD15^{hi}CD66b^{hi}$ surface marker expression.

2.2.3   FACS sorting of LDGs

PBMC from the patient and healthy donors were incubated with fluorochrome conjugated antibodies against surface CD14 for 30 minutes on ice, followed by two washing steps with wash media at 300g and 4°C for 10 minutes. Next, CD14 negative cells were separated from the population in on a cell sorter (BD FACS Melody™) and differentiated into two fractions according to their FSC-SSC proportions. As LDGs are the largest and most granular cell population, the fraction with the higher FSC-SSC dimension was then further utilized in downstream experiments.

2.2.4   Neutrophil Labelling with Dihydrorhodamine 123

Neutrophils were left untreated or were treated with PMA as a positive control for 15 minutes at 37°C in the presence of DHR123. As neutrophils are short-lived and susceptible to activation, the cells were placed on ice immediately at the end of the incubation period. Reactive oxygen species (ROS) analysis was carried out with flow cytometry, where untreated healthy neutrophils were used as baseline for DHR123 positivity.

2.2.5   PBMC Stimulations

Freshly isolated PBMC were layered into tissue culture treated flat-bottom clear 96-well plates at a density of 400,000 cells/well in 100μl of culture medium. TLR agonists were added according to their working concentrations given in Table 2.2 in 100μl, completing the total volume of each well to 200μl. Ligands that require cytosolic delivery were first mixed with 0.3μl/well Lipofectamine™ 2000 Transfection Reagent (Thermo Fisher Scientific, #11668019) and completed to 50μl with FBS free Opti-MEM (Thermo Fisher Scientific, #31985070). The mixture was then incubated 5-10 minutes at room temperature to allow complexation and completed to full volume with culture media prior to transfection. Following the addition of stimulants, the plates were incubated at 37°C for 24 hours and subsequently centrifuged at 250g and room temperature for 10 minutes to collect the supernatant without cellular debris. The supernatants were stored at -20°C until their utilization in downstream experiments. For assessment of protein ISGylation and free ISG15 determination, PBMCs were stimulated overnight as positive controls in the presence of HSV60 or IFN-β at 37°C.

2.2.6   Cytokine Quantification

The IL-1β, IL-6, IFN-γ, IFN-α(pan), and IP-10 cytokine levels secreted from patient and healthy PBMC were quantified using the ELISA kits listed in Table 2.4. First, 50μl/well of capture antibodies at a concentration recommended by the manufacturer were incubated overnight at 4°C in polystyrene treated semi-hydrophobic 96-well flat bottom plates. The coating solution was discarded by rapid inversion of the plate, and then plates were blocked at room temperature for 2 hours with 200μl/well of blocking buffer (Appendix A). Next, the blocking buffer was discarded again by rapid inversion and the plates were soaked in wash buffer (Appendix A) 5 times each for 3 minutes. Then, 50μl/well culture supernatants were added and the plates were incubated at room temperature for 2 hours. Afterwards, the plates were washed again as described above. Biotin labelled detection antibodies were added at 50μl/well at a concentration recommended by the manufacturer and the plates were incubated overnight at 4°C. The plates were washed once more as previously described and 1:1000 diluted alkaline phosphatase (ALP) or horseradish peroxidase (HRP) conjugated streptavidin was added at 50μl/well. Following incubation at room temperature for 1 hour, the plates were washed again and enzyme substrates PNPP for ALP or TMB for HRP was added at a volume of 50μl/well. The plates were incubated in dark and color development was monitored at 5minute intervals. Spectrophotometric measurements were taken for ALP activity at 30minute intervals at 405nm wavelength, while HRP activity was stopped with H_2SO_4 after color development and measured at 450nm. Alternatively, IP-10 quantification was performed with cytometric bead array (CBA, BD Biosciences #558280) according to the manufacturer's protocol.

2.2.7   Lysate Preparation and Immunoblotting

Freshly isolated or stimulated PBMC (4×10^6) were centrifuged at 300g at room temperature for 10 minutes and subsequently resuspended in 40μl ($20\mu l/1 \times 10^6$ cells)

of mammalian protein extraction reagent (M-PER, Thermo Fisher Scientific #78501). The suspension was incubated on ice for 30 minutes while vortexing every 10 minute to ensure proper lysis. Afterwards, the samples were spun at 14,000g at 4°C for 15 minutes and the supernatant was collected and stored at -80°C for further SDS-PAGE and western blot applications.

Protein quantification was carried out using the micro BCA™ Protein Assay Kit (Thermo Fisher Scientific, #23235) according to the manufacturer's instructions. 30μg of protein extract was mixed with SDS containing loading buffer (Appendix A) at a ratio of 1:6. The sample volumes were completed to 25μl with dH_2O and incubated at 95°C for 5 minutes. At the end of the incubation, the tubes were put promptly on ice and subsequently were briefly spun to collect the liquid evaporated to the lid. Next, the samples were loaded separately into the wells of a 4-15% gradient precast polyacrylamide protein gel (BioRAD, #4568083). Molecular weight confirmation was achieved by loading a pre-stained protein ladder of 1-180kDa (Thermo Fisher Scientific, #26616) into one well. The tank was filled with running buffer (Appendix A) and electrophoresis was performed with a constant voltage of 120V for 1-1.5 hours. Transfer of proteins from the gel to a nitrocellulose membrane was carried out by preparing a stack of transfer components in the following order; sponge-sponge-filter paper-protein gel-nitrocellulose membrane- filter paper-sponge-sponge. After the pack was placed into the transfer cassette, the reservoir was filled with transfer buffer (Appendix A) and the electrophoretic conditions were set at 30V for 1 hour. Next, the nitrocellulose membrane carrying the proteins was washed once with TBS-T (Appendix A) and subsequently placed into blocking buffer (Appendix A) for 1 hour at room temperature. Then, the membrane was washed with TBS-T five times, each for 5 minutes and put into TBS-T containing a primary antibody (1:500 dilution) and incubated overnight at 4°C. Following another washing step at the previously described conditions, the membrane was placed into TBS-T containing the HRP conjugated secondary antibody (1:3000 dilution) for 1 hour at room temperature. After another washing step, the chemiluminescence reaction was induced with the Clarity Western ECL substrate (BioRAD, #1705061)

and imaged with the ChemiDoc XRS+ system. Image Lab software was used for densitometric analysis of the protein bands. Normalization was performed by taking the proportion of the densitometric intensity acquired for the protein of interest to each individual GAPDH band intensity. Secondary normalizations were carried out by dividing each normalized density to the mean of healthy controls.

2.2.8 RNA Isolation

Freshly isolated 4×10^6 PBMC or neutrophils were centrifuged at 300g at room temperature for 10 minutes and thoroughly resuspended in 1ml of Trizol™ reagent until the cell pellet disappeared, indicating complete lysis. The samples were stored as such at -80°C until all time points were collected to perform side by side RNA isolation.

Frozen Trizol™ samples were thawed first on ice, then incubated at room temperature for 5 minutes. Next, 200µl of chloroform was added to 1ml of Trizol™ and mixed thoroughly using a vortex. The samples were then incubated at room temperature for 3 minutes and subsequently centrifuged at 12,000g and 4°C for 15 minutes. Phase separation into 3 layers was observed. At least 500µl from the RNA rich aqueous phase was collected into RNase free 1.5ml tubes without contact to the white colored DNA containing interphase. Isopropanol was added to the aqueous phase at a 1:1 ratio. The tubes were inverted gently 10 times and incubated at room temperature for 10 minutes. After centrifugation at 12,000g and 4°C for 10 minutes, the supernatant was aspirated leaving the white RNA pellet. Next, 1ml of 99.8% ethanol (Sigma-Aldrich, #32221) was added so that the pellet became detached and washed without breaking. The samples were spun at 8000g for 8 minutes and similarly washed again with 70% ethanol. Alternatively, RNA isolation was performed with the RNA Clean & Concentrator kit after collecting the RNA rich aqueous phase according to the manufacturer's instructions. Following resuspension with 25µl of RNase free dH_2O, RNA quantity and quality were assessed using the BioDrop (BioChrom) spectrophotometer.

2.2.9   Nanostring Gene Expression Analysis

For gene expression analysis, 50μg of RNA was mixed with the reporter code sets from the corresponding panel according to the manufacturer's suggestions. Next, the hybridization reaction was initiated and run overnight at constant 65°C in a thermal cycler (LongGene® MyGene™ L Series Peltier Thermal Cycler or BioRAD T100™ Thermal Cycler). The hybridized RNA samples were then put into the nanoString® workstation instrument for the automated cartridge loading procedure. After the samples were fixed to the bottom, the cartridge was placed into the analyzer device to obtain raw transcript counts. The counts were then normalized according to internal housekeeping gene expression provided in the panel. The resulting data was used to analyze differential gene expression on the baseline of healthy control expressions in the nSolver Analysis Software 4.0.

CHAPTER 3

RESULTS AND DISCUSSION

PART ONE

3.1 Intrinsic and Functional Verification of NEMO deficiency

The nuclear factor (NF) – κB essential modulator (NEMO, IKK-γ) is a protein subunit of the inhibitor of κB kinase (IKK) complex located in the cytosol (Häcker & Karin, 2006). The heterotrimeric complex consists of the catalytic subunits IKK-α and IKK-β, while IKK-γ takes up a regulatory role (Sun & Ley, 2008). The IKK complex phosphorylates the inhibitor of κB (IκB) that is bound to the NF-κB transcription factor (Hayden & Ghosh, 2008). The phosphorylation of IκB leads to its rapid ubiquitylation and subsequent degradation, while NF-κB is uninhibited and translocates into the nucleus (Baeuerle & Baltimore, 1988). NF-κB activity is essential for the initiation of innate and adaptive immune responses as well as the regulation of proliferative and apoptotic pathways (A. R. Liu & Ramakrishnan, 2021). Its absence results in embryonic lethality in males while females develop incontinentia pigmenti (IP) (Smahl et al., 2000). Hypomorphic mutations in males, on the other hand, lead to ectodermal dysplasia (EDA) with immune deficiency (EDA-ID) (Ramírez-Alejo et al., 2015).

The NEMO deficiency patient presented with ectodermal developmental anomalies such as conical teeth, sparse hair and eyebrows, and hyperpigmentation of the skin. Additionally, the patient also had a history of recurrent infections, including with CMV and *Mycobacterium tuberculosis*. Targeted next-generation sequencing (NGS) revealed a stop codon (p.Gln205*; NM_001093327) as a consequence of a previously reported nonsense mutation (c.613C>T; NM_001099857.5) in the *IKBKG* gene (Klemann et al., 2016). Paradoxically, the patient also displayed

autoinflammatory manifestations such as interstitial and perivascular neutrophilic infiltrations, subcutaneous swelling, and painful nodular skin lesions. In this study, we aimed to gain insight into the underlying mechanistic events leading to severe clinical autoinflammation in NEMO deficiency.

First, in order to intrinsically verify the genetic analysis, we ran an SDS-PAGE followed by immunoblotting against the N-terminus (240-419 a.a.) of the 419 amino acid NEMO protein using PBMC lysates from the patient, the father, and healthy unrelated individuals. While healthy controls and the father of the patient expectedly displayed two bands, one at 48kDa and the second for the isoform at around 42kDa, no bands were detected in the patient's PBMC lysate before HSCT (Figure 3.1). As the initial antibody was specific to the region after the stop codon, our immunoblot confirmed the absence of an intact NEMO protein in the patient. 9-months after HSCT, a NEMO-specific band was visible (Figure 3.1; right panel), indicating that bone marrow transplantation successfully reconstituted the defective protein.
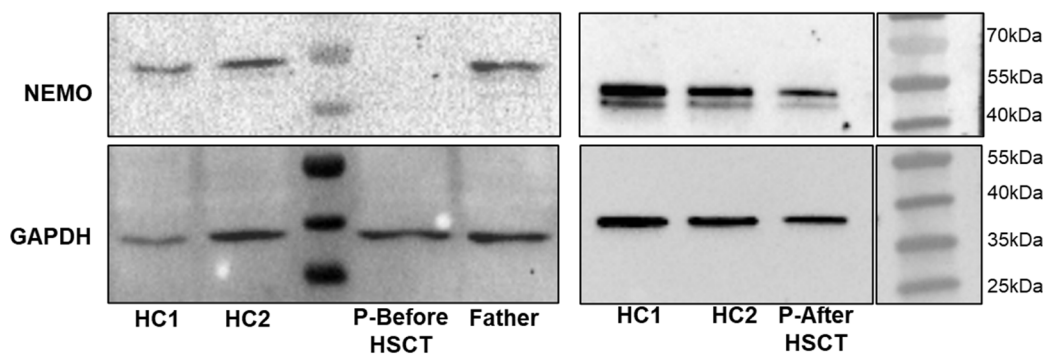
Figure 3.1 Verification of NEMO deficiency. Immunoblotting images of anti-NEMO and anti-GAPDH before (left) and after (right) the patient underwent HSCT. Sample identifications are indicated at the bottom. Molecular weights are denoted on the right. HC1: Healthy 1; HC2: Healthy 2; Father: Father of the patient; P-Before HSCT: Patient sample before HSCT; P-After HSCT: Patient sample after HSCT.
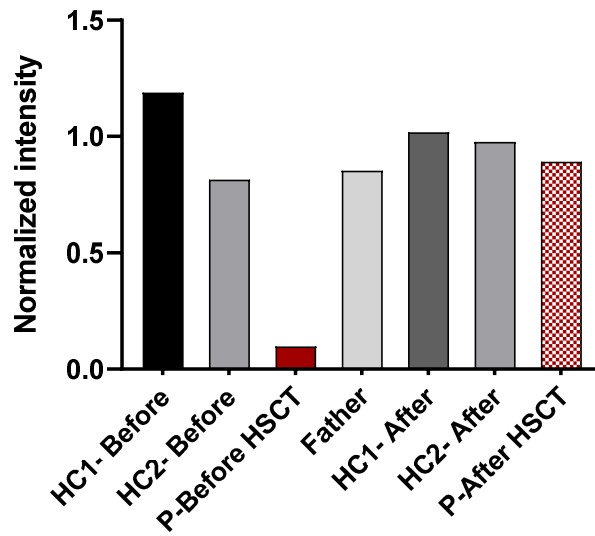
Figure 3.1 (cont'd): Normalized densitometric analysis of the anti-NEMO immunoblot..

The c.613C>T; NM_001099857.5 nonsense mutation was previously documented by Klemann et al., who showed the absence of the 48kDa intact protein, but at the same time an abundance of the 40kDa isoform. We tried to replicate this observation with our patient and used two alternative antibodies, one specific to the C-terminus (1-150 a.a.) and the other against the full-length NEMO protein. However, probing against the C-terminal end resulted in the same outcome, neither the 48kDa protein nor the lower molecular weight isoform was detectable in the sample from the patient prior to HSCT, while both bands were clearly visible in the sample obtained after transplantation as well as in healthy control lysates (Figure 3.2).
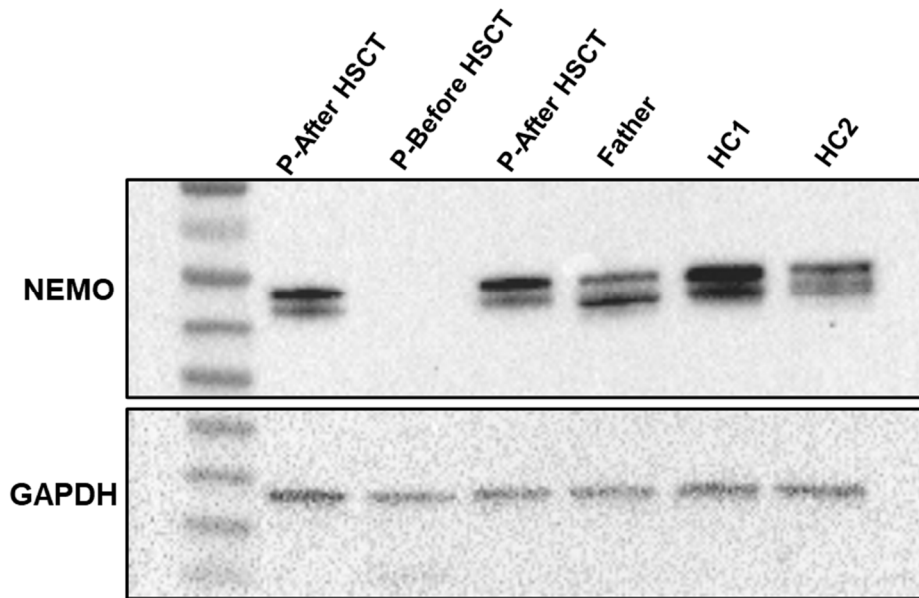
Figure 3.2 Immunoblot images of C-terminus specific anti-NEMO and anti-GAPDH. Sample identifications are indicated at the top.

These results contradict with the earlier observation by Klemann et al.. Nevertheless, we hypothesize that if the patient did in fact utilize an isoform of NEMO or a shorter truncated protein, it might have been exposed to rapid proteasomal degradation, as the patient was in a highly autoinflammatory state. Unfortunately, the patient PBMC lysate from before transplantation was already used up at this point. Therefore, to test the full-length antibody, we obtained a puncture biopsy skin sample from the patient since transplantation only involves the replacement of the hematopoietic lineage but not the skin allowing for analysis of the mutant NEMO in the skin tissue even after transplantation. We prepared a single cell suspension from the biopsy sample using a tissue dissociator and subsequently performed protein extraction. The biopsy sample came in a container with residual red blood cells, which we also used for lysate preparation. We performed another immunoblotting experiment against full-length NEMO and as we could not obtain a healthy skin biopsy, we compared both patient samples to healthy PBMC lysates. Even though all samples were

GAPDH positive, we could not detect NEMO in either of the patient samples (Figure 3.3).
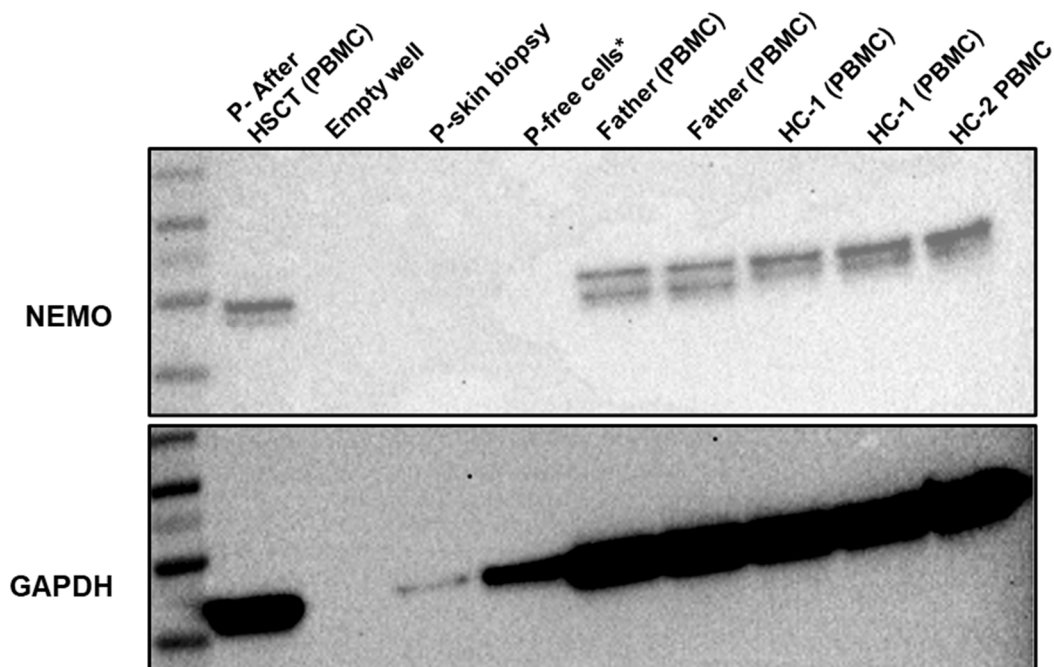
Figure 3.3 Immunoblot images of full-length anti-NEMO and anti-GAPDH. Sample identifications are indicated at the top.

Our immunoblotting experiments demonstrated the absence of an intact NEMO protein in the patient. However, we know from preceeding literature that the complete lack of NEMO should be embryonically lethal in males. We believe that our inability to identify a truncated version of the mutated NEMO might be associated with the detection method we employed. In consideration of the sample integrity, truncated proteins are more readily susceptible to degradation, and therefore it may not be suitable to select western blotting as the detection method. As we did not posess any frozen patient cells before HSCT, our inability to detect a short truncated protein or another isoform of NEMO generated through alternative splicing as was suggested by Klemann et al, remains as a limitation of this study.

After establishing the deficiency of NEMO in the patient, we tried to understand the extent of the resulting immunological functional impairment. Extracellular as well as intracellular stimuli can activate the NF-κB pathway by signaling through the IKK complex. Toll-like receptors (TLRs), vital sensors of the innate immune system, are either bound to the outer membrane or endosomal membranes of immune cells. While TLR1, TLR2, TLR4, TLR5, and TLR6 reside on the outer plasma membrane; TLR3, TLR7, TLR8, and TLR9 are located on endosomal membranes (Kawai & Akira, 2007). The activation of these receptors triggers IKK to phosphorylate IκB, thereby releasing NF-κB to travel into the nucleus and initiate pro-inflammatory gene expression. In this context, we treated PBMC of the patient and healthy controls with diverse TLR agonists and measured IL-1β and IL-6 cytokine secretion as a consequence of NF-κB activation. Furthermore, signaling through the cytosolic dsDNA sensing cGAS-STING pathway also leads to the recruitment and activation of the IKK complex and subsequent NF-κB induced gene expression. We observed that PBMC from the patient prior to transplantation were not able to produce IL-1β and IL-6 as efficiently as healthy controls in response to TLR and cGAS activation, while the response of patient cells to the same agonists were normalized to healthy levels post-HSCT (Figure 3.4).

In addition to its functions within the innate immune system, effector cell activation of the adaptive immune system is highly dependent on NF-κB signaling as well. T-cells require NF-κB activation for clonal expansion and differentiation to their effector subtypes such as Th1, Th17, Treg, while B-cells need NF-κB activity for proliferation, germinal center formation, and differentiation into antibody producing plasma cells (Hsia, Cheng, Owyang, Dowdy, & Liou, 2002). In order to assess T-cell receptor (TCR) activation independent but Protein kinase C-directed NF-KB- and calcium-mediated IFN-γ release from Th1/CD8 T cells, we treated PBMC from the patient and healthy controls with PMA/ionomycin before and after HSCT. Our results revealed that the patient cells were not able to produce IFN-γ when compared to healthy PBMC prior to transplantation, but secreted this cytokine at levels similar to healthy controls post-HSCT (Figure 3.5).
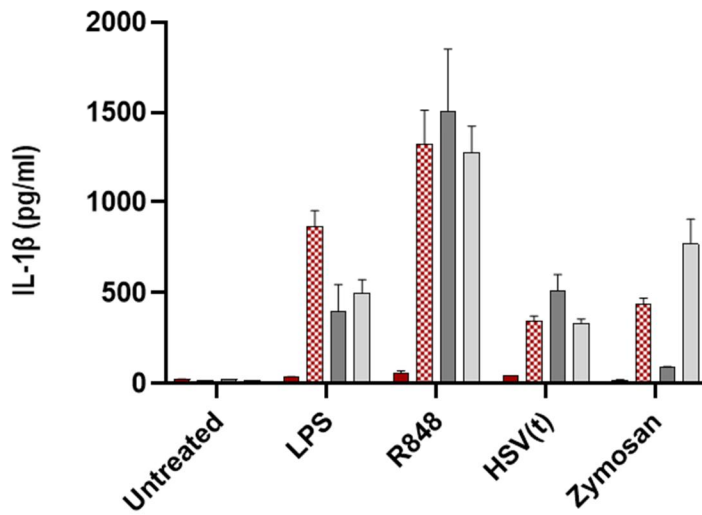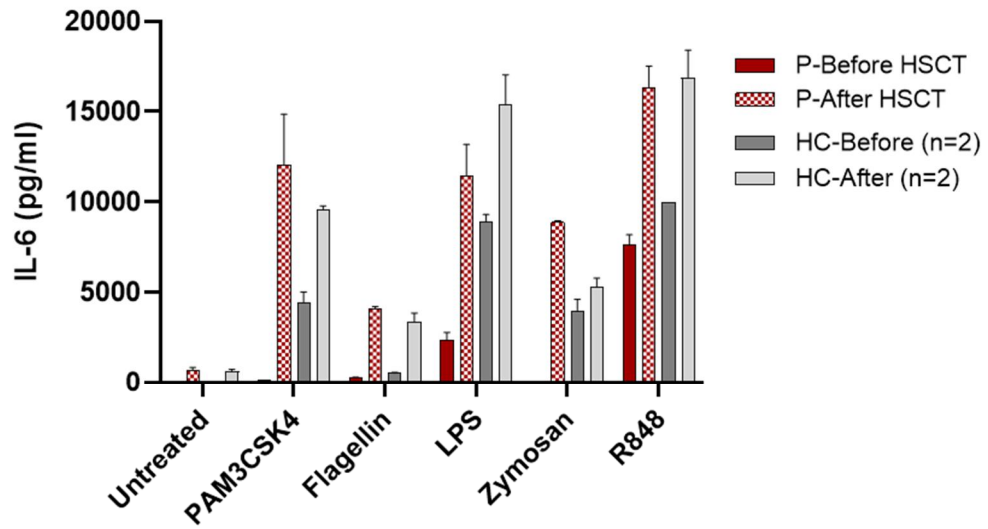
Figure 3.4 Bar graphs of IL-6 and IL-1β ELISA quantifications from culture supernatants of PBMCs stimulated for 24 hour with the following ligands: PAM3CSK4: TLR1/2; flagellin: TLR5; LPS: TLR4; zymosan: TLR5; R848: TLR 7/8; HSV60 (Herpes simplex virus 60bp dsDNA): cGAS-STING. (P: patient; HC: healthy control)
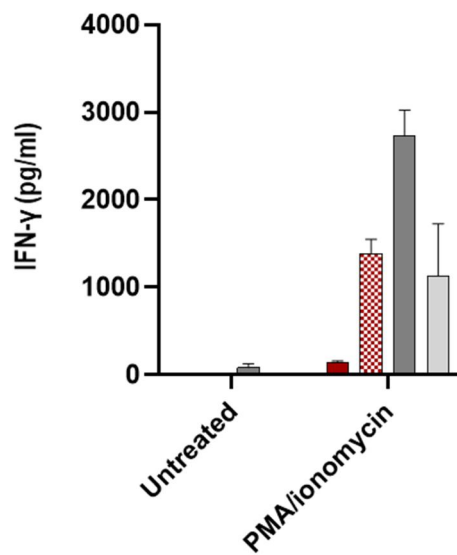
Figure 3.5 : Bar graph of IFN-γ ELISA quantification from the culture supernatant of NEMO deficient or healthy PBMCs stimulated for 24 hours without or with PMA/ionomycin (P: patient; HC: healthy control)

Our results demonstrate, that due to the absence of intact NEMO proteins before HSCT, the patient was unable to respond to inflammatory stimuli as efficiently as healthy individuals. Specifically, the patient failed to secrete the pro-inflammatory cytokines IL-6 and IL-1β in response to TLR ligand stimulation or intracellular dsDNA, suggesting severe impairment in innate immune recognition of PAMPs. Furthermore, the patient failed to exhibit sufficient IFN-γ production following NF-KB activation, showing incomplete signal transduction and gene expression in T-cells. Up to this point, we established that NEMO deficient PBMCs from the patient were unable to initiate fundamental innate or adaptive immune activation, explaining the recurrent infections that the patient experienced before undergoing HSCT.

3.2   Baseline Gene Expression Analysis Reveals the Presence of Inflammatory Granulocytes in PBMC fraction

In order to study the contribution of possible mechanisms that might explain the chronic inflammation-mediated pathology seen in the patient before HSCT, we utilized the nanoString® Inflammation and PanCancer Immune Profiling gene expression panels comprised of 225 and 730 genes, respectively. While the Inflammation panel was used directly before the patient underwent transplantation, the PanCancer Immune Profiling panel was utilized with samples both before and after transplantation. In coherence with the clinical immune deficiency, the patient exhibited significant downregulation of innate effector genes such as *nlrp3*, *il1a*, *il1b*, and *il6* (Figures 3.6; 3.7; 3.8). In a healthy system, the expression of these genes in PBMC would be expected to increase following NF-κB activation and return to their baseline levels after the resolution of inflammation. Our data demonstrate that baseline levels of innate effector molecule expression was reduced in the patient compared to healthy PBMC. Given that the patient is unable to induce complete NF-κB activation, it is possible that NEMO deficient PBMCs prioritize resource regulation away from redundant NF-KB-related inflammatory pathways through epigenetic modifications.

Interestingly, the analyses from both gene expression panels revealed increased expression of genes specific to a granulocytic origin, at the same time showing elevated levels of inflammation promoting genes (Figures 3.6; 3.7; 3.8). According to the Inflammation panel analysis, the patient exhibited the highest differential upregulation with the *mmp9* gene levels (Figures 3.6; 3.8), which is mostly expressed in neutrophils, encoding for matrix metalloprotease-9. This enzyme enables the degradation of the extracellular matrix (ECM) in order for neutrophils to navigate through tissues towards the site of infection/inflammation (Mayadas, Cullere, & Lowell, 2014). Moreover, *arg1* is constitutively expressed in neutrophils and was also upregulated in NEMO deficient PBMC (Figures 3.6; 3.8). Its product arginase-1, is stored in azurophilic granules of neutrophils until activation and release for

antimicrobial activity (Mayadas et al., 2014). Additionally, the *defa1* gene. encoding for the cytotoxic peptide Neutrophil Defensin 1, was also observed to be elevated in the patient before HSCT (Figure 3.8).

P-Before vs HC
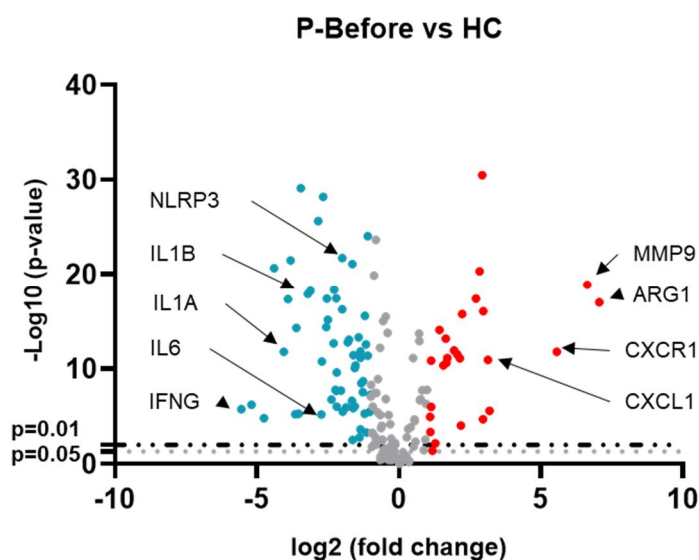
Figure 3.6 Volcano plot of differentially expressed Inflammation panel genes between NEMO deficient and healthy PBMC. Red dots: fold change ≥ 2; blue dots: fold change ≤ 2. Dashed line: P=0.01; dotted line: P=0.05. Corresponding gene names are indicated with black arrows.

Further analysis conducted with the PanCancer Immune Profiling panel, later supported our initial findings validating the elevated expression of granulocyte-specific and inflammation associated genes. Strikingly, the *ltf* gene, encoding for lactoferrin, another antimicrobial protein stored in neutrophil granules (Kruzel, Zimecki, & Actor, 2017), showed the highest upregulation in NEMO deficient PBMC (Figures 3.7; 3.8). Moreover, another antimicrobial protein capable of limiting bacterial growth known as neutrophil gelatinase associated lipocalin-2 (LCN2), was found to be significantly elevated in the patient before HSCT (Figures 3.7; 3.8). Other neutrophil specific genes known as *s100a12* and *s100a8* were also among the most abundantly expressed genes compared to healthy controls (Figures 3.7; 3.8). Furthermore, the expression of *ceacam8*, encoding for another surface

antigen that is normally expected on activated neutrophils was also observed to be enhanced prior to transplantation (Figures 3.7; 3.8).
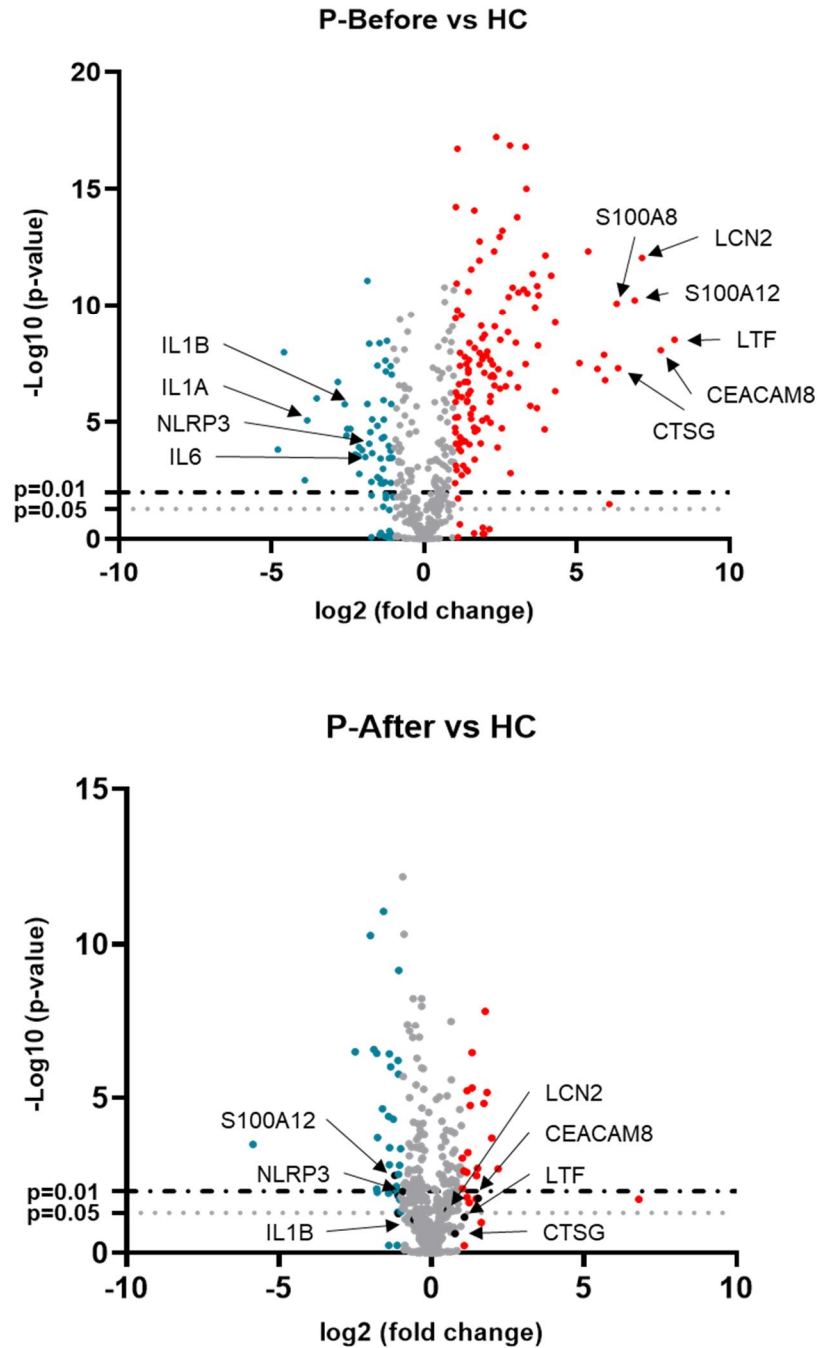
Figure 3.7 Volcano plot of differentially expressed PanCancer Immune Profiling panel genes between healthy and NEMO deficient (Top) or NEMO reconstituted (Bottom) PBMC. Red dots: fold change ≥ 2; blue dots: fold change ≤ 2. Dashed line: P=0.01; dotted line: P=0.05. Corresponding gene names are indicated with black arrows.
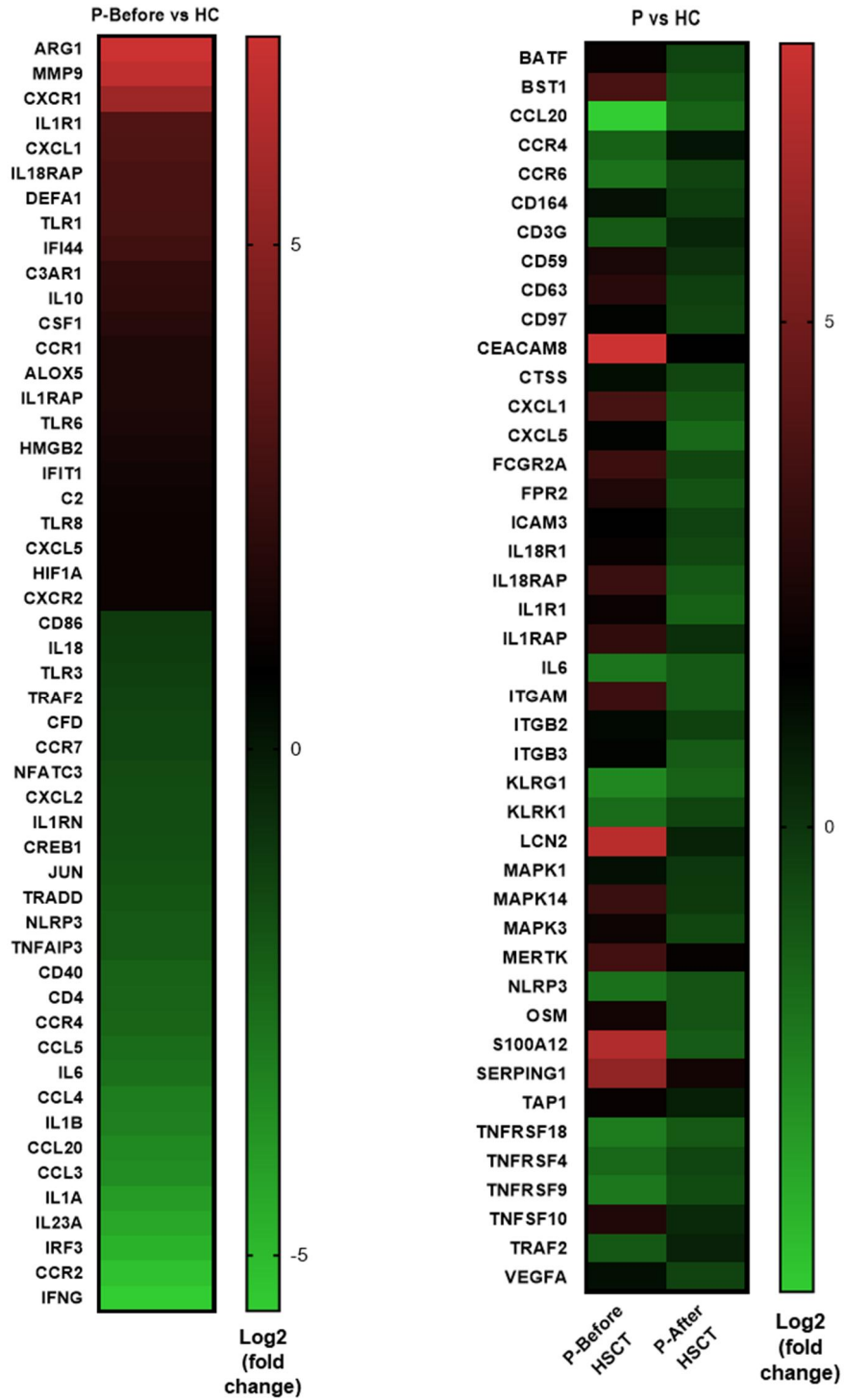
Figure 3.8 Heatmaps of differentially expressed genes between NEMO deficient and healthy PBMC using the Inflammation (Left) and PanCancer Immune Profiling (Right) gene panels. Fold changes are calculated on the baseline of healthy control. (P: patient; HC: healthy control)

To avoid limiting our evaluation on single genes, we also looked at the up/downregulation patterns of gene groups associated with different immunological functions. Pathway enrichment analysis expectedly showed elevated expression of adhesion, chemokine, macrophage and leukocyte function associated gene groups before the patient underwent HSCT (Figures 3.9; 3.10).

Figure 3.9 Horizontal bar graphs for z-scores of target gene groups. Scores are calculated from the differential expression of corresponding genes for adhesion (upper left), chemokines (upper right), macrophage functions (lower left), and leukocyte functions (lower right). (P: patient; HC: healthy control)

We reasoned that the increased expression of the gene groups for macrophage and leukocyte functions as well as antigen processing and pathogen defense is in line with the chronic tissue inflammation the patient had been experiencing (Figures 3.9; 3.10). Tissue damage would also mean elevated expression and release of cytokines

and chemokines which further recruits immune cells to the inflamed region. These cells then, would require to upregulate adhesion related gene groups to infiltrate the target site, which is in parallel with the clinically observed interstitial and perivascular neutrophilic infiltrations. Furthermore, chronic autoinflammation in the patient also explains the elevated expression of cell cycle and senescence related genes due to accelerated production and maturation of immune cells (Figure 3.10). However, we observed downregulation of gene groups associated with T-cell and NK cell functions, as well as in groups related to cytotoxicity and interleukins (Figure 3.10). Here, we think that the absence of NEMO protein function, leads to an interference with the expression of these gene groups as cellular functions like cytotoxicity and interleukin production are highly dependent on NF-κB activity.

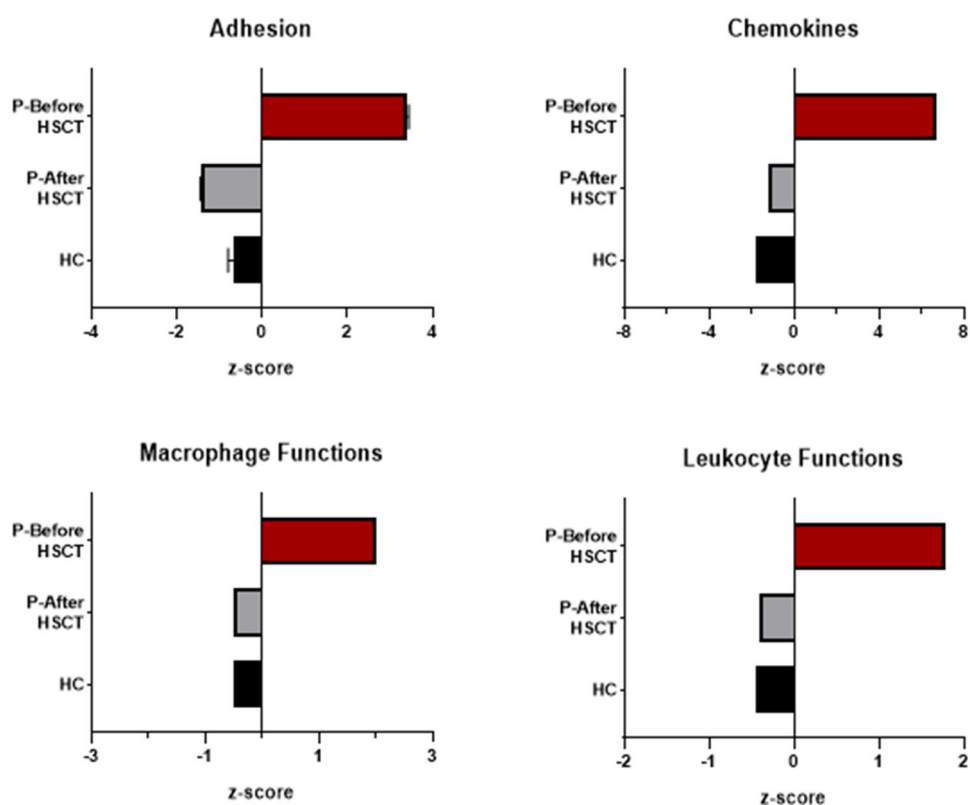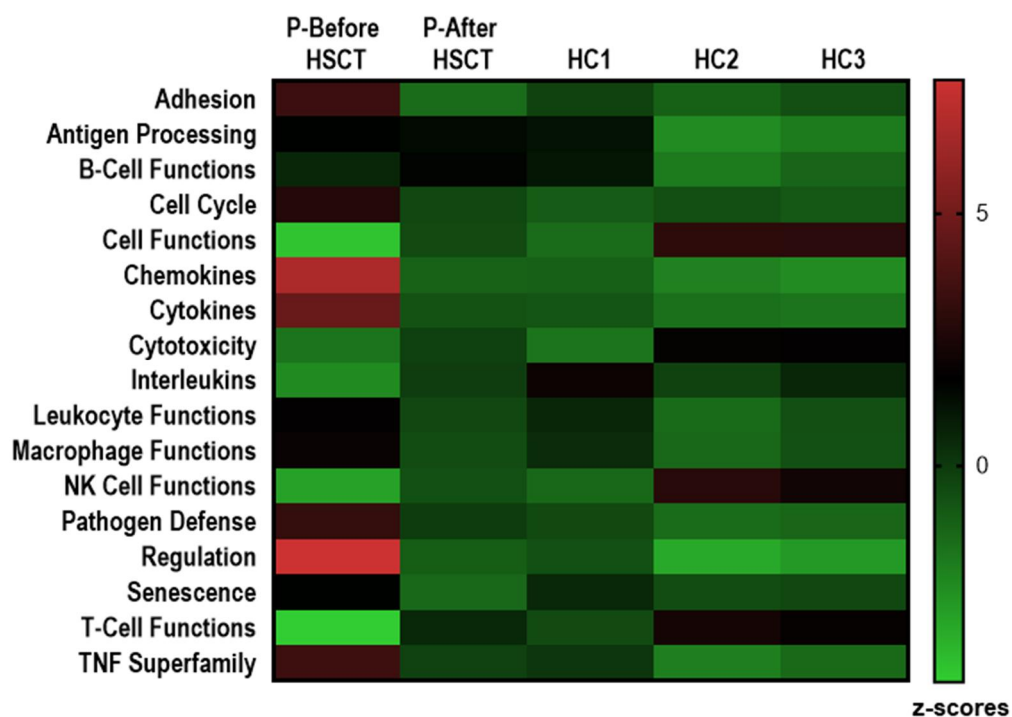*Figure 3.10 Heatmap for z-scores of listed gene groups. Scores are calculated from the differential expression of corresponding genes for each functional group.*

The results obtained from PBMC after the patient underwent HSCT shows normalization of gene expression to levels similar to healthy controls, which is consistent with the improvement of the patient's clinical symptoms. Collectively, our data indicate the presence of activated cells of granulocytic origin that potentially inflict persistent tissue damage prior to HSCT.

3.3 Identification of Increased frequency of LDG population in the NEMO deficient patient

Consistent with the elevated gene expression related to activated granulocytes, we detected an unusually large and granular cell population in the PBMC fraction of blood from the patient. Later, through cell surface marker staining, we were able to identify that these cells were low-density granulocytes (LDG). This distinctive cell population was first characterized by Denny et al. in systemic lupus erythematosus (SLE) patients as inflammatory granulocytes that are prematurely released from the bone marrow and capable of inflicting tissue damage (Denny et al., 2010). In order to identify whether the granulocytic population in the patient were in fact LDG, we labelled PBMC from the patient and healthy individuals with fluorochrome conjugated antibodies against cell surface differentiation markers. Cells originating from a granulocytic lineage abundantly express the surface antigen CD15, while the monocytic marker CD14 is displayed quite dimly. Moreover, CD66b is another surface marker that can be observed on activated neutrophils, differentiating these cells from the resting neutrophil population. In this context, we used fluorescence conjugated anti-CD14, anti-CD15, and anti-CD66b antibodies and analyzed the PBMC from the patient and healthy controls using flow cytometry. While healthy individuals expectedly had 0-2% LDG in their PBMC, the patient had 34-35% of LDG in the PBMC fraction before undergoing transplantation (Figure 3.11). Importantly, we obtained a similar outcome when we repeated this experiment after five months, suggesting that the autoinflammatory state of the patient was not an acute but a chronic condition until HSCT (Figure 3.11). However, stainings that were

performed after the HSCT showed the gradual disappearance of the LDG, which is in parallel with the subsiding clinical autoinflammatory manifestations.
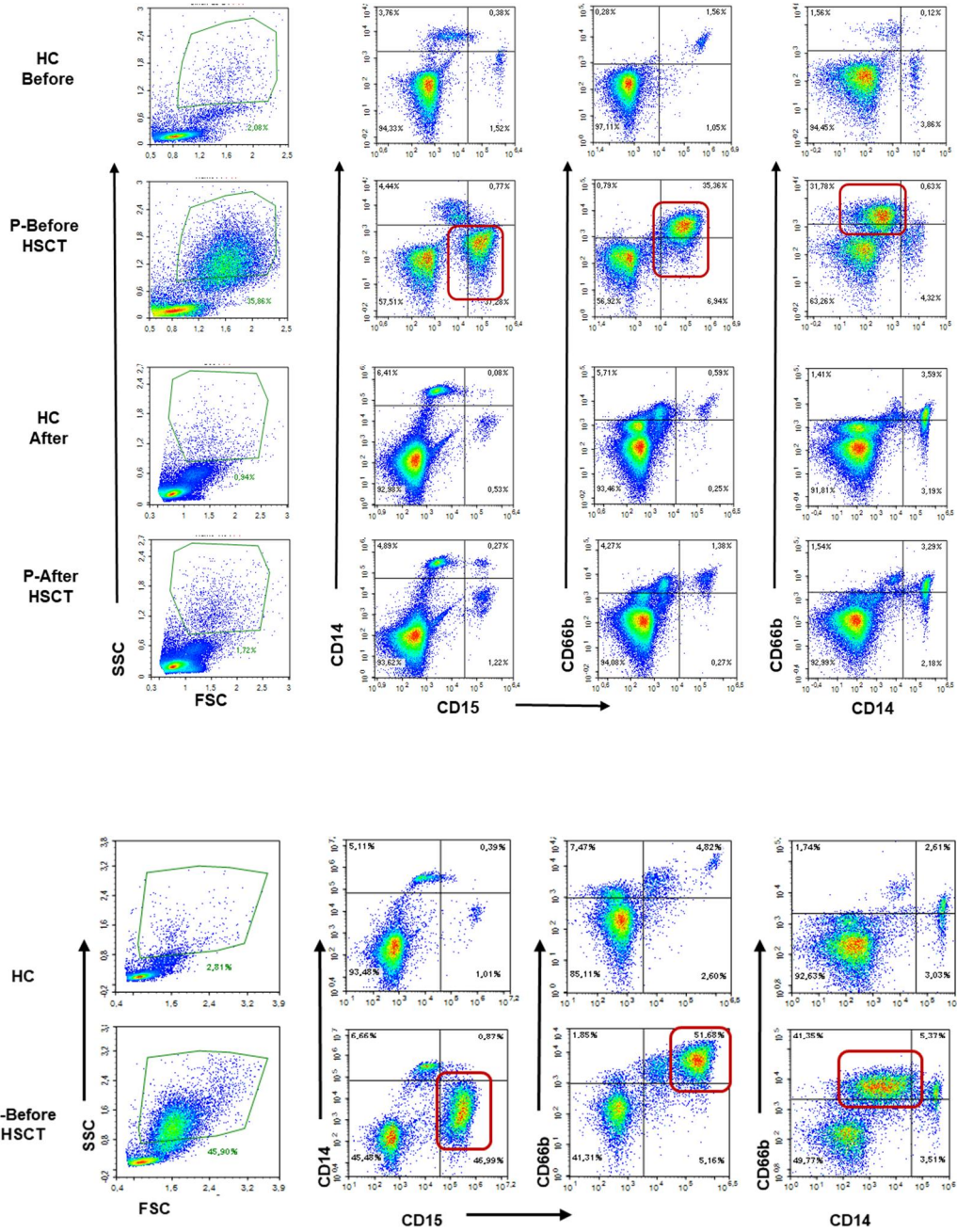
Figure 3.11 Flow cytometry density plots and gating strategy to identify LDG in PBMC from the patient before and after HSCT compared to healthy PBMC. Staining experiments before and after transplantation were conducted at different time points from freshly isolated PBMC but are displayed together for ease of comparison. LDG detection before transplantation was conducted two times 5 months apart (top and bottom panels).

Of note, increase of the surface antigen CD66b was also observed at the gene expression level showing at least 200-fold higher *ceacam8* transcripts in the patient (Figures 3.7; 3.8), further supporting the finding of increased LDG in the patient.

3.4 Identification of Neutrophil dysregulation in the NEMO deficient patient

Since the presence of LDG points to atypical neutrophil development, we also examined normal density neutrophils from the patient and compared their activation status to healthy neutrophils. Activated neutrophils generate reactive oxygen species (ROS) through the enzymatic activity of NADPH-oxidase as a downstream defense mechanism against pathogenic invaders. Therefore, as an indicator of their activation state, we compared the superoxide content of freshly isolated neutrophils from the patient and healthy control.

Within this scope, untreated or PMA treated NEMO deficient or healthy neutrophils were labelled with the membrane-permeable non-fluorescent compound dihydrorhodamine123 (DHR123), which emits green fluorescence upon oxidation. Subsequent flow cytometric analysis revealed that the patient had 40% more ROS positive untreated neutrophils than healthy controls, suggesting that NEMO deficient resting neutrophils from the patient were in a spontaneously primed state relative to healthy neutrophils (Figures 3.12; 3.13). Neutrophils that were treated with PMA as a positive control were found 99% ROS positive in both groups (Figures 3.12; 3.13).
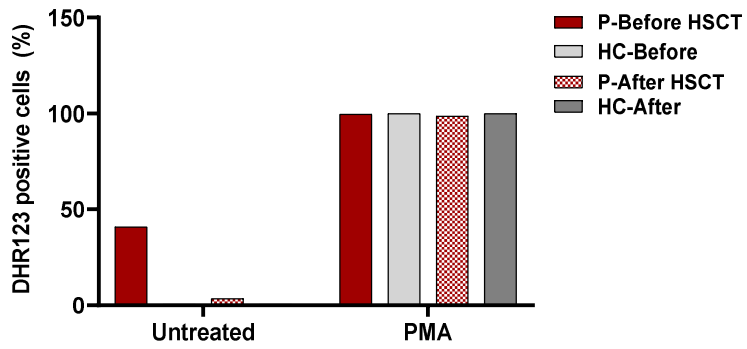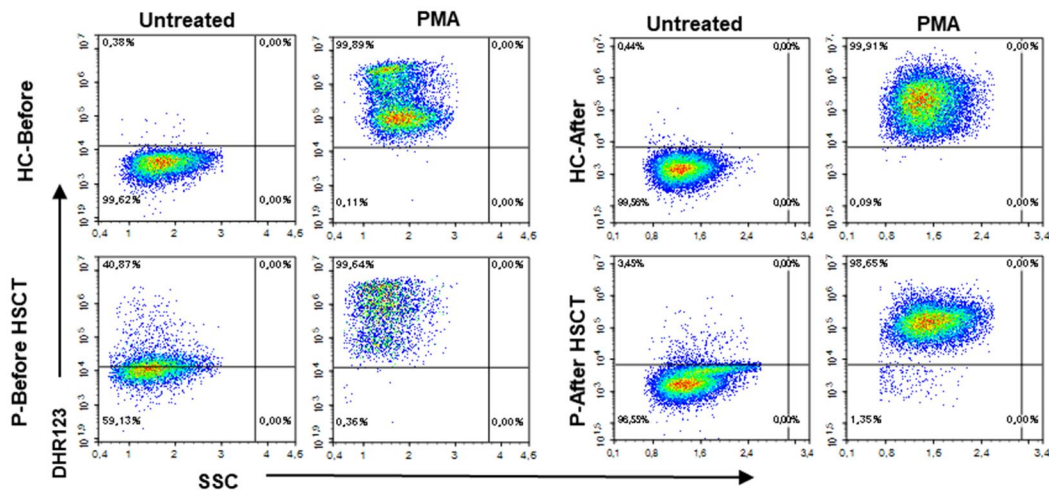
Figure 3.12 Flow cytometric analysis of reactive oxygen species generation in neutrophils. Density plots (top) and bar graphs (bottom) of DHR-123 fluorescence as indicative of ROS generation in NEMO deficient or healthy neutrophils without or with PMA stimulation are shown. . (P: patient; HC: healthy control)
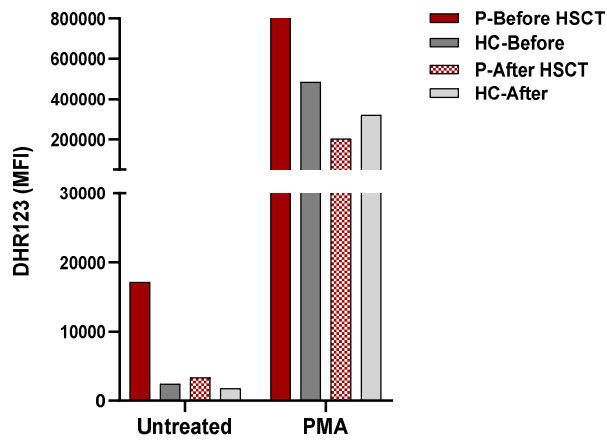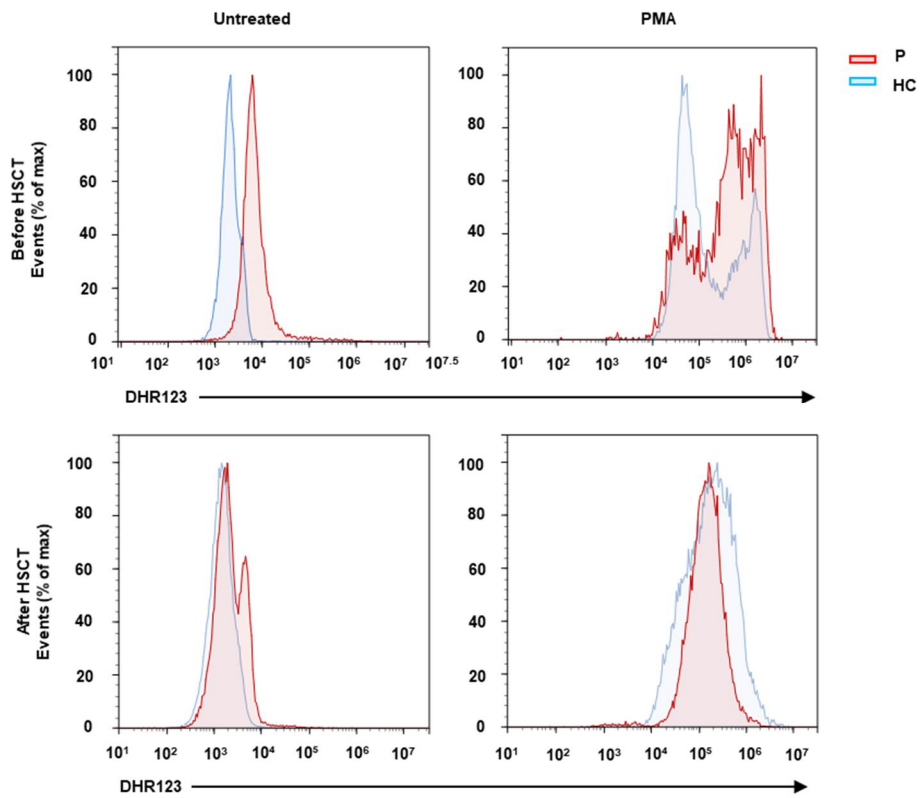
Figure 3.13 Flow cytometric analysis of reactive oxygen species generation in neutrophils. Histograms (top) and bar graphs (bottom) of DHR-123 MFI (mean fluorescence intensity) as indicative of ROS generation in NEMO deficient or healthy neutrophils without or with PMA stimulation are shown. (P: patient; HC: healthy control)

In order to better understand the cellular mechanism(s) leading to autoinflammatory pathology, we examined the gene expression profiles of LDGs and normal density neutrophils of NEMO deficient patient in comparison to healthy neutrophils. Our results show upregulation of inflammation associated genes in patient neutrophils, including the adhesion proteins ceacam1, ceacam6, and ceacam8. Furthermore, we observed substantial fold increase in expression of the antimicrobial genes *ltf* (~870 fold) and *lcn2* (~330 fold) in LDG, suggesting activation of inflammatory gene expression pathways (Figures 3.14; 3.15). Additionally, we found that the *cybb* encoding for p91-phox, a subunit of the NADPH-oxidase complex, was significantly upregulated in LDG (Figures 3.14; 3.15) Finally, the genes *ctsg* and *ctsh*, encoding for neutrophilic peptidase and lysosomal cysteine protease, respectively were also upregulated (Figures 3.14; 3.15).
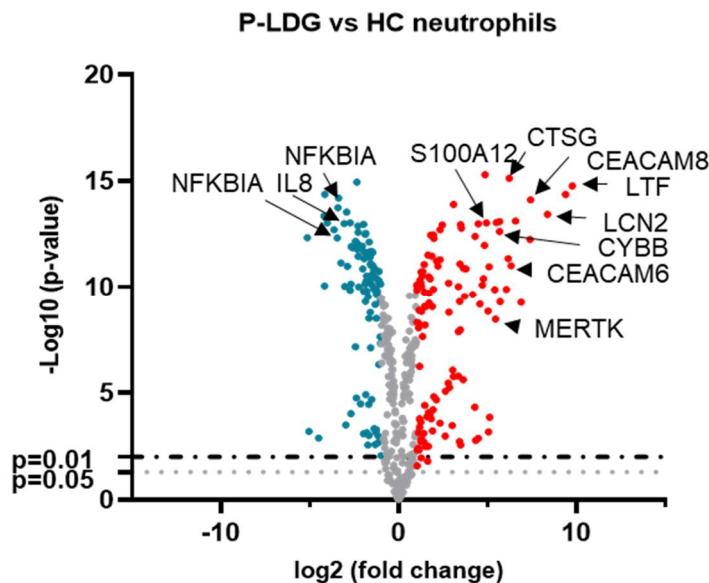
Figure 3.14 Volcano plot of differentially expressed PanCancer Immune Profiling panel genes between patient LDG and healthy neutrophils. Red dots: fold change ≥ 2; blue dots: fold change ≤ 2. Dashed line: P=0.01; dotted line: P=0.05. Corresponding gene names are indicated with black arrows.

A similar pattern of gene upregulation was observed in NEMO deficient neutrophils vs healthy controls (Figure 3.15), although this difference was less pronounced

compared to LDGs. Patient neutrophils displayed elevated levels of adhesion associated genes as well as genes responsible for orchestrating antimicrobial defense. However, genes belonging to the IL-1 and IL-1R families were downregulated in both LDG and NEMO deficient neutrophils (Figure 3.15), possibly due to the immune deficieny.
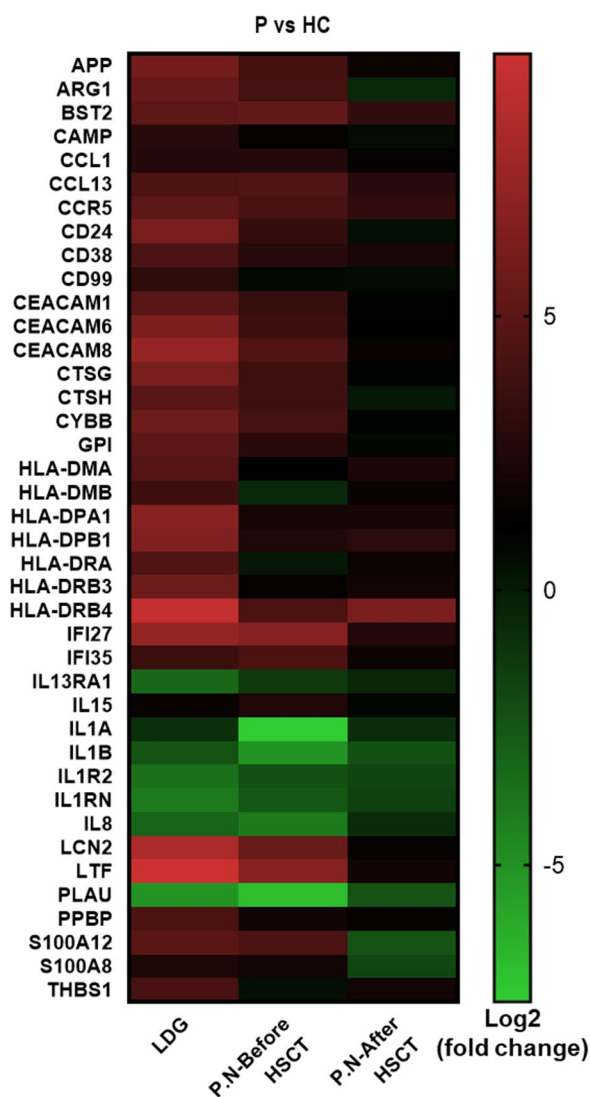
Figure 3.15 Heatmap of log2 fold changes of differentially expressed genes in LDG, NEMO deficient and NEMO reconstituted neutrophils with respect to healthy control using the PanCancer Immune Profiling gene panel. (P.N: patient neutrophils; HC: healthy control)

Neutrophils are the first responders to a site of infection and therefore activate pathways that enable their egress from circulation into the tissue and instigate inflammatory damage. With respect to different gene groups, LDG show the most increase in adhesion and cell functions (Figure 3.16) related genes, strengthening the view that LDG actively contribute to tissue damage. Moreover, we observed elevation in gene groups related to senescence and transporter functions as well (Figure 3.16). As senescent cells release cytokines and chemokines to the environment, they can potentially exacerbate inflammation. Furthermore, activated neutrophils need to mobilize intracellular granules for degranulation, thereby explaining the increased expression of genes regulating transporter functions.
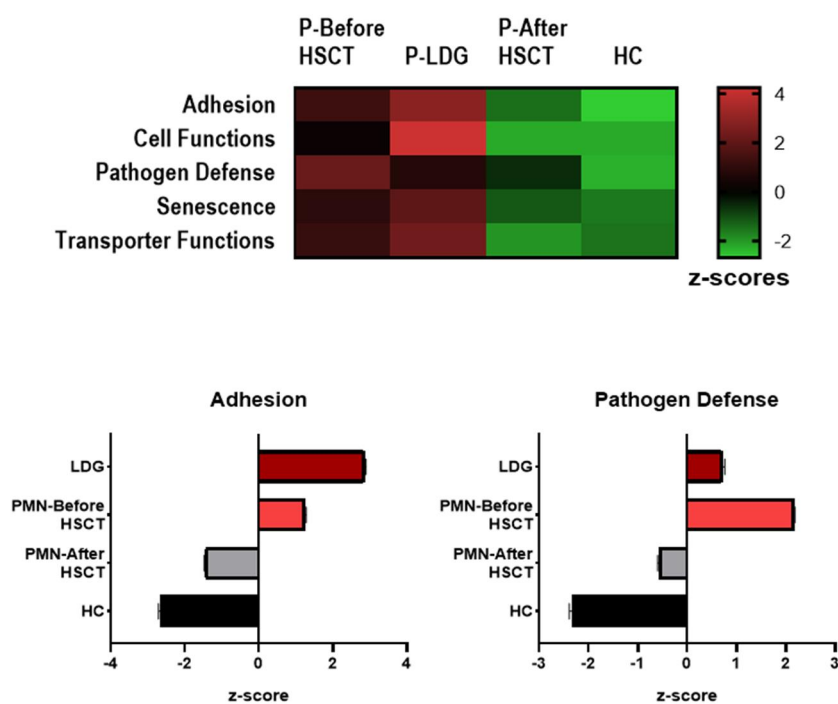
Figure 3.16 Gene expression analysis results as heatmap(top) and horizontal bar graphs (bottom) for z-scores of listed gene groups. Scores are calculated from the differential expression of corresponding genes for each functional group. (P: patient; HC: healthy control)

Collectively, our functional and gene expression data from the patient prior to HSCT, indicate that inflammatory LDGs and primed neutrophils are equipped with cellular changes enabling them to infiltrate tissues, causing damage. The fact that the clinical autoinflammatory manifestations subsided in keeping with the disappearance of LDGs and primed neutrophils post-HSCT, points to their involvement in the pathophysiology.

3.5   Identification of Spontaneous Type I IFN Signature in NEMO deficient patient cells

As the spontaneous presence of LDG and primed neutrophils is highly unexpected in an immune deficient patient, we sought to investigate what might be causing the dysregulation of granulocyte development and maturation in NEMO deficiency. It has been reported previously that type I IFNs can have a stimulatory effect on neutrophils in autoinflammatory conditions (Gul et al., 2018). In order to explore whether a similar mechanism operates in NEMO deficiency, we tested for evidence of elevated type I IFN signature in the circulation by measuring IP-10 (CXCL10, IFN-γ inducible protein 10) levels from the patient plasma. IP-10 is a cytokine that is released as a result of type I or type II IFN secretion and signaling. CBA (cytometric bead array) analysis for IP-10 revealed an excessive amount of IP-10 in the patient compared to healthy plasma, which was later confirmed with ELISA (Figure 3.17). Furthermore, IFNα ELISA from plasma also demonstrated around 3-fold higher levels in the patient than in healthy control (Figure 3.17).
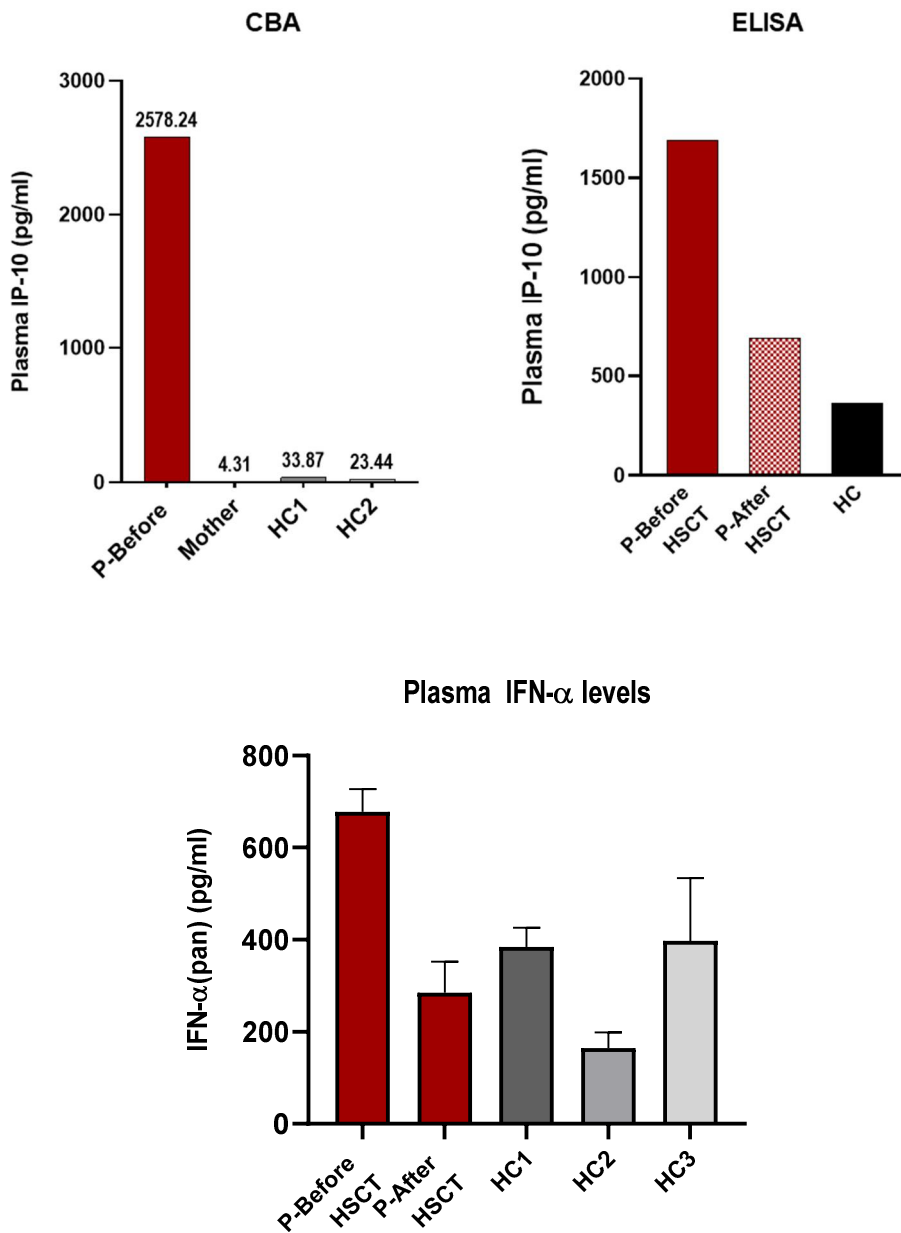
Figure 3.17 Bar graphs illustrating cytokine levels IP-10 (top) and IFN-α (bottom) in plasma obtained from healthy controls and the patient. Upper left: CBA (cytometric bead array), upper right: ELISA (enzyme linked immunosorbent assay) (P: patient; HC: healthy control)

To verify that type I interferon signature was indeed elevated in the patient, we used PBMC lysates from the patient and healthy controls to blot against ISG15, which is a ubiquitin-like protein that can be covalently bound to cellular proteins in response

to type I IFN signaling in a process known as ISGylation. Moreover, ISG15 can act as a cytokine in its free form either in the intracellular environment or extracellularly (Perng & Lenschow, 2018). Immunoblotting experiments revealed spontaneous heavy ISGylation of PBMC proteins and the presence of free ISG15 in patient protein extracts that disappeared after the patient underwent HSCT (Figure 3.18).
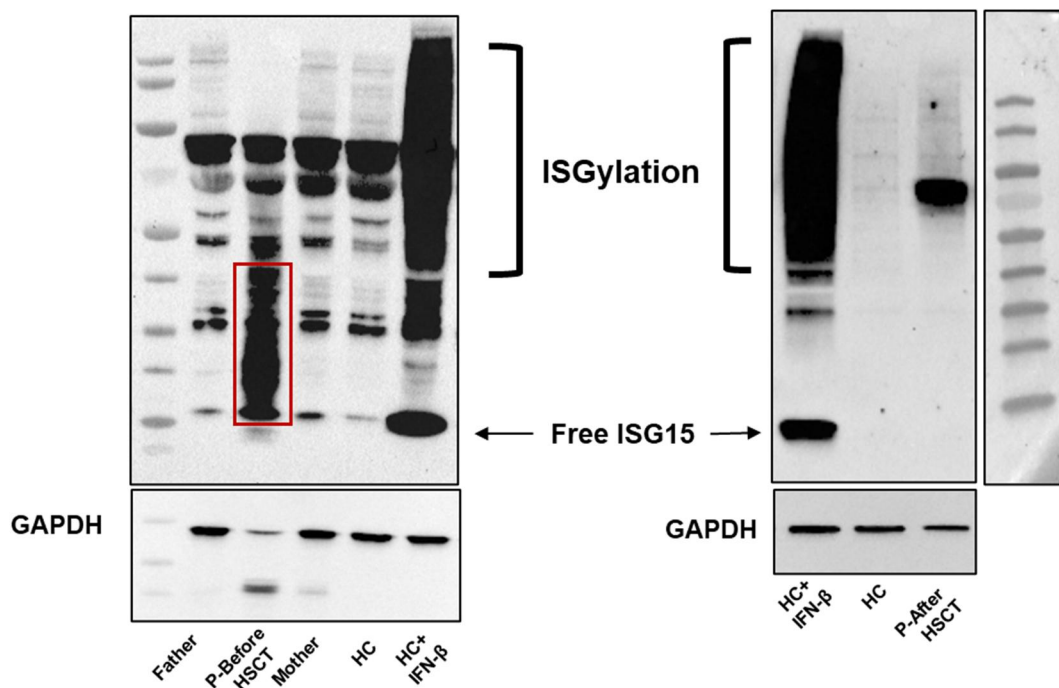
Figure 3.18 Immunoblot images of anti-ISG15 and anti-GAPDH. Left panel shows images obtained before transplantation, right panel shows images taken from experiments conducted post-transplantation. Red rectangle in the left image indicates the ISGylation pattern in NEMO deficient PBMC. Sample identifications are indicated at the bottom. (P: patient; HC: healthy control)

Elevated IP-10 and IFN-α levels in the plasma together with the ISGylation pattern found in PBMC demonstrates that the patient exhibited a type I IFN signature in the absence of an acute infection. These data are supported by the elevated expression of interferon response genes such as *isg15* (17-fold), *mx1* (6-fold), *oas3* (19-fold) as well as *cxcl10* (~5 fold), *ifit1* (~12 fold), *ifi35* (~13 fold) in PBMC of the patient prior to HSCT (Figure 3.19). Since the disappearance of LDG and the primed

neutrophil populations overlap with the decrease in type I IFN as well as with the clinical improvement of the patient, it is likely that the autoinflammatory manifestations in the patient were the result of a spontaneous IFN signature causing dysregulation in granulocyte activity.
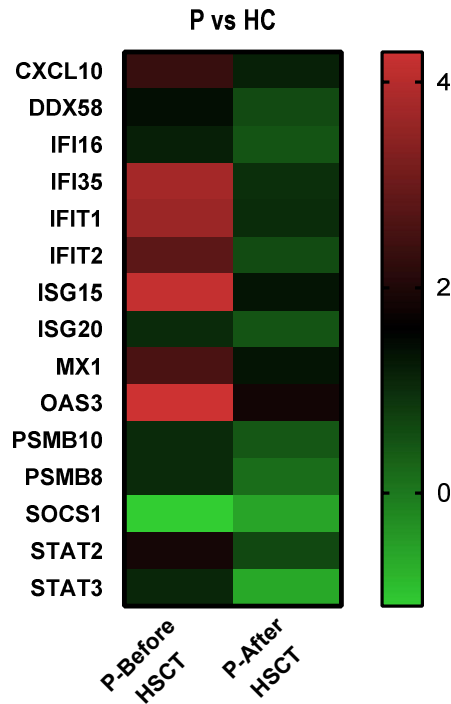
Figure 3.19 Heatmap of IFN response related differentially expressed genes in NEMO deficient or NEMO reconstituted PBMC with respect to healthy PBMC. (P: patient; HC: healthy control)

Of interest, we detected multiple bands of housekeeping proteins in immunoblot images obtained with patient PBMC lysates, indicative of protein degradation (Figure X). Neutrophils carry granules containing high amounts of inhibitor resistant proteases capable of ECM degradation, enabling the cells to migrate through tissues as part of the immediate innate immune defense. Given that the patient exhibits 99-fold increase in the expression of MMP9 (matrix metalloprotease 9) (Figure 3.6), we reasoned that the presence of excess inflammatory LDG in the PBMC and their

release of resilient granular proteases, might have led to partial protein degradation in the course of lysate preparation. In order to avoid the possibility that NEMO might have been degraded by proteases originating from LDGs, we depleted monocytes and LDGs from the PBMC population and repeated lysate preparation and probing against NEMO and ISG15. Immunoblotting shows that NEMO is still absent in the patient compared to healthy control, thereby proving that LDG originating proteases did not cause the absence of NEMO-specific band (Figure 3.20).
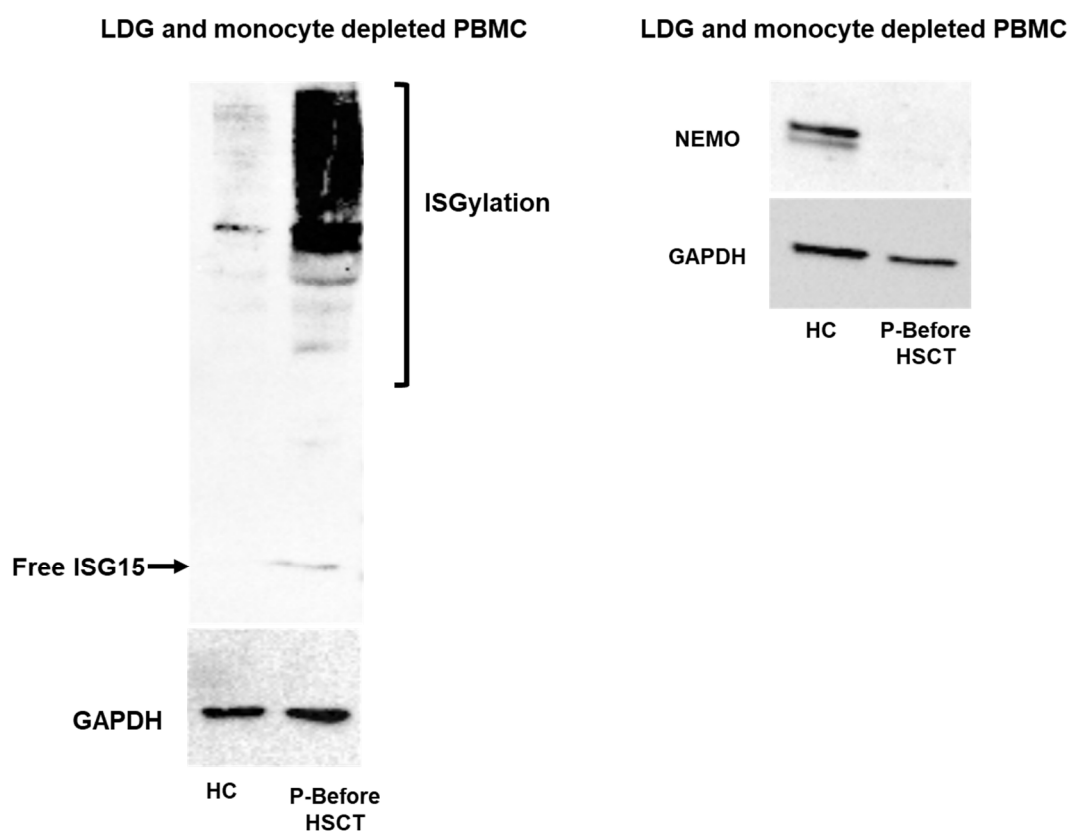
Figure 3.20 Immunoblot images illustrating probing against anti-ISG15 (left) and anti-NEMO (right) in LDG and monocyte depleted PBMC populations before transplantation. (P: patient; HC: healthy control)

Furthermore, probing against ISG15 demonstrates ISGylation of cellular proteins in the patient even after LDG and monocyte depletion (Figure 3.20). The fact that other

PBMC components show an ISGylation pattern, supports the notion that the type I IFN response in the patient is a systemic event and not solely LDG dependent. Of note, the depletion experiments were conducted five months apart from the initial immunoblots, again providing evidence for the chronic autoinflammatory status of the patient.

Collectively, our results illustrate that spontaneous type I IFN signature in NEMO deficiency might have led to premature granulocyte release from the bone marrow and dysregulation of neutrophil activity, causing severe systemic autoinflammation in the patient only amendable through HSCT.

CHAPTER 4

RESULTS AND DISCUSSION

PART TWO

4.1 The Inflammatory Gene Expression Environment Improves with Abatacept Therapy in CHAI and LATAIE Patients

Human inborn errors of immunity CHAI and LATAIE, formerly known as CTLA-4 haploinsufficiency and LRBA deficiencies, respectively, unite in their clinical phenotypes as both disorders arise due to the lack of CTLA-4 on the plasma membrane of regulatory and activated T-cells. CTLA-4 is a small ~23kDa inhibitory protein able to compete with the CD28 receptor for binding with the co-stimulatory B7 (CD80 and CD86) ligands on antigen presenting cells. The LRBA protein, as detailed in section 1.2.2, has been identified to be responsible for the prevention of premature lysosomal degradation of CTLA-4 through interacting with its cytoplasmic tail domain. Common clinical features of CHAI and LATAIE include lymphocyte overactivation and infiltration of non-lymphoid tissues, autoimmune cytopenia, lymphadenopathy, hypogammaglobulinemia. The latter symptom has been found counterintuitive, especially as mouse models display elevated antibody levels. While experiments involving mice take place in an infection-controlled environment, patients are constantly exposed to pathogens. Therefore, it has been postulated that the persistent stimulation of B-cells causes their exhaustion, as evidenced by $CD21^{lo}$ B-cell counts, potentially explaining the hypogammaglobulinemia. Furthermore, patients suffering from unregulated lymphoproliferation, as is the case in CHAI and LATAIE, can become prone to developing lymphoma. However, as CHAI originates from CTLA-4 haploinsufficiency, but LATAIE results from the absence of the LRBA protein, some

variation of their clinical symptoms in spite of their similarities have also been documented embodied in the severity and time of onset of the disease.

In order to investigate potential underlying mechanisms that govern the pathophysiology observed in CHAI and LATAIE patients and to examine the effect of abatacept therapy at the gene expression level, we performed a transcriptome analysis using the Human Host Response gene expression panel from the PBMC that were isolated before and after the patients started receiving therapy. We obtained samples before treatment, three months, eight months, and twelve months afterwards. Our initial comparison of baseline expression levels in CHAI patients to healthy control revealed upregulation in chemotaxis associated genes such as *cxcl3*, *cxcl1*, and *cxcl10* encoding for the corresponding chemokines CXCL1, CXCL3, and CXCL10 (IP-10) (Figures 4.1; 4.2). The latter is known as the IFN-γ inducible protein 10 (IP-10) and is produced upon type I and type II IFN signaling. CXCL1 and CXCL3 are important mediators for the recruitment of neutrophils and have been associated with angiogenesis in the tumor microenvironment. Furthermore, gene expression analysis displayed increase in neutrophil granular antimicrobial proteins such as *defa4*¸ *lcn2*, and *bpi*, encoding for alpha defensin 4, neutrophil gelatinase associated lipocalin 2, and bactericidal permeability increasing protein, respectively (Figure 4.2). These are antimicrobial peptides found in primary or secondary granules of neutrophils, which are released upon activation for pathogen killing. Moreover, genes of the IL1 receptor family, *il1r1* and *il1r2*, were enhanced in CHAI patients (Figure 4.2). Additionally, interferon inducible genes encoding for guanylate binding proteins (GBP) such as *gbp1* and *gbp5* were elevated as well (Figure 4.2). GBP5 has also been shown to take part in the assembly of the NLRP3 inflammasome. The expression of genes *tigit* and *havcr2*, encoding for surface proteins that are found on T_{FH} and T_H1 subclasses, respectively, were also increased (Figure 4.2). While the product of *tigit*, the T-cell immunoreceptor with Ig and ITIM domains, has been associated with T-cell exhaustion in liver cancer, *havcr2* encoding Hepatitis A Virus Cellular Receptor 2 has been reported to promote immunological tolerance.
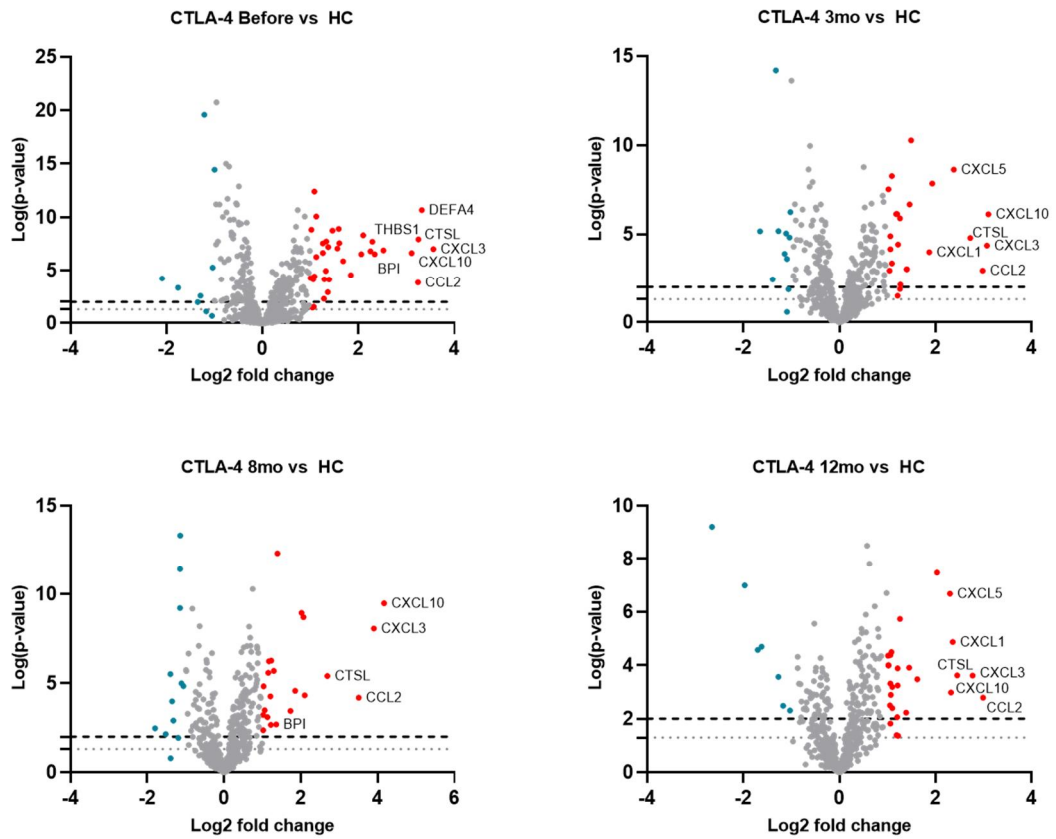
Figure 4.1 Volcano plot of differentially expressed Host Response panel genes between healthy and CHAI patient PBMC before therapy (upper left), after 3months (upper right), 8 months (lower left), and 12 months (lower right). Red dots: fold change ≥ 2; blue dots: fold change ≤ 2. Dashed line: P=0.01; dotted line: P=0.05.

CTLA-4 vs HC
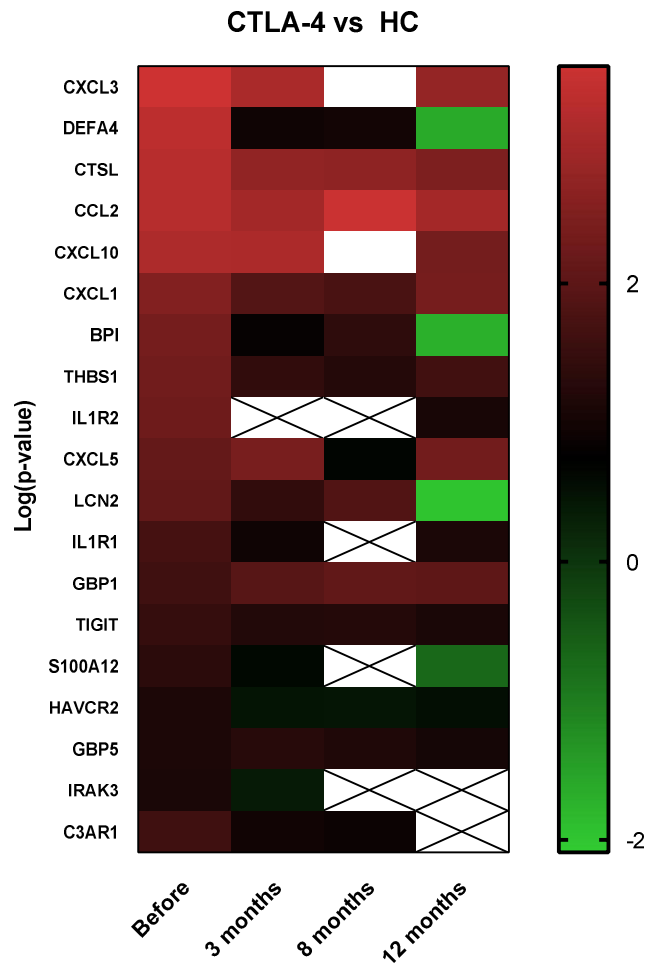
Figure 4.2 Heatmap of differentially expressed genes between healthy and CHAI patient PBMC before therapy, after 3 months, 8 months, and 12 months using the Host Response gene panel. Fold changes are calculated on the baseline of healthy control. Data points with P<0.05 were excluded. (P: patient; HC: healthy control)

The increased expression of chemokine signaling related genes complemented with elevated levels of the *thbs1* gene (Figure 4.2), encoding for thrombospondin 1, a protein associated with cellular ECM interactions and able to bind integrins, can be explained by the lymphocytic infiltrations observed in CHAI patients. As a consequence of this intrusion and the overactivation of especially CD8^{+} cytotoxic T-cells on site causing damage to the surrounding tissue, other resident immune cells such as macrophages or dendritic cells would be expected to become stimulated. Of

note, the uncontrolled and persistent activity of T-cells might explain the elevation of genes associated with immune exhaustion. This would lead to the secretion of more inflammatory mediators resulting in further recruitment and activation of monocytes and neutrophils, possibly accounting for the increased levels of neutrophil specific antimicrobial peptide expression. In parallel, the existent tissue damage releasing host derived danger molecules (DAMPs) into the extracellular environment, thereby activating TLR and NLR pathways might have led to the enhanced levels of IL1 and NF-κB related genes. Additionally, host associated molecules would also include DNA and RNA motifs, activating sensing mechanisms that trigger type I and II IFN pathways.

The comparison between healthy controls and CHAI patients that started receiving abatacept therapy, demonstrate that neutrophil originating host defense peptide expressions were reduced at least after 3 months and were still normalized at 12 months (Figure 4.2). Similarly, our results show that IL1 signaling associated gene expression was reduced to healthy levels also at least after 3 months of treatment. Additionally, we observed that *thbs1* expression was downregulated after 3 months and 8 months, but slightly increased at 12 months, yet not as much as at the baseline level (Figure 4.2). Furthermore, the expression of exhaustion associated genes *tigit* and *havcr2* also were reduced starting at 3 months and remained normalized up to 12 months (Figure 4.2). Altogether, this data suggests that abatacept treatment seems effective in preventing lymphocyte overactivation. However, chemotaxis related gene expression levels were still elevated at all time points after the beginning of therapy (Figure 4.1; 4.2).

Expectedly, LATAIE patients displayed similar upregulation patterns as CHAI patients (Figure 4.3; 4.4). We observed increased levels of neutrophil specific genes such as *lcn2* and *defa4* as compared to healthy controls, which also normalized at least after 3 and 8 months of receiving abatacept, respectively (Figure 4.4). Similarly, IL1 signaling associated *il1r2* was elevated before treatment, but reduced to healthy expression levels starting at 8 months and remained downregulated up to 12 months (Figure 4.4). LATAIE patients also displayed upregulation of GBP encoding genes

like *gbp1* and *gbp5*, however, expression levels persisted throughout all time points for both disease groups compared to healthy controls (Figure 4.4). Despite many similarities in expression patterns, LATAIE patients also show variation in upregulated genes. Interestingly, we observed the highest differential expression in the apoptosis associated *bcl2l1* gene encoding for the Bcl-x protein with long (Bcl-x_L) and short (Bcl-x_S) isoforms harboring opposite functions (Figure 4.3; 4.4). After the beginning of abatacept therapy, the expression of this gene gradually decreases starting at 3 months and normalizing at 8 months (Figure 4.4). Further supporting the relation of LRBA with apoptosis and autophagy, we detected elevated expression of the *mt2a* gene as well, encoding for metallothionein 2A, involved in metal metabolism (Figure 4.4).
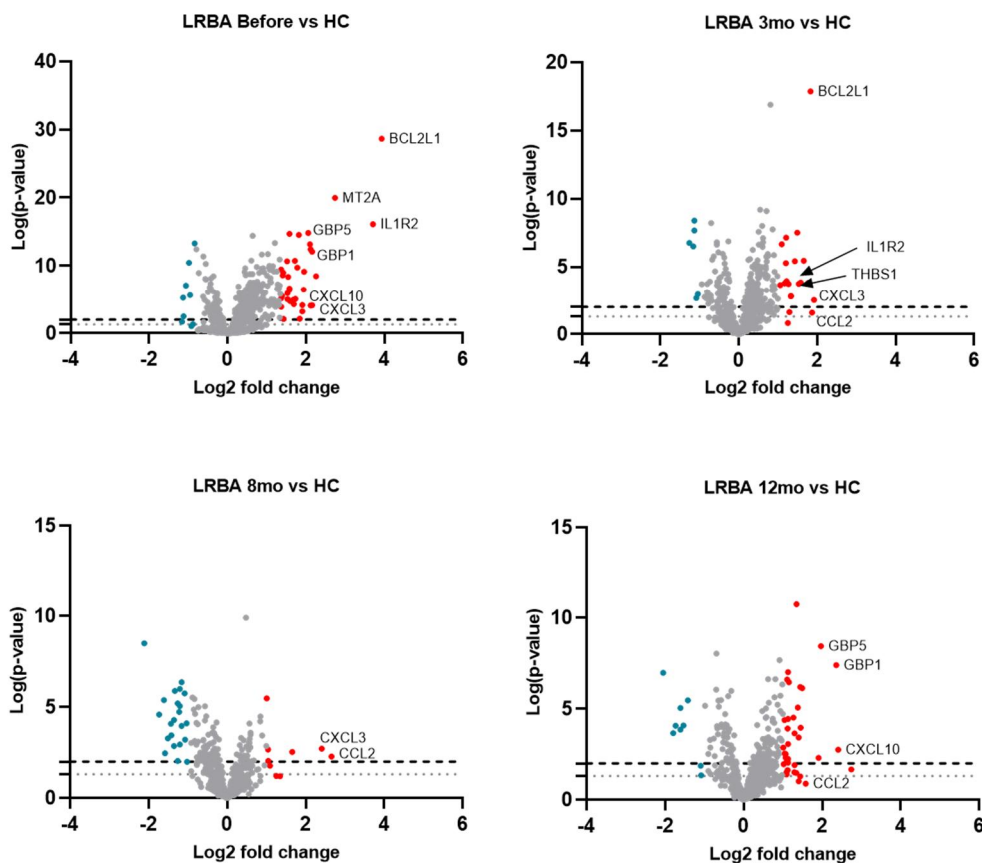
Figure 4.3 Volcano plot of differentially expressed Host Response panel genes between healthy and LATAIE (LRBA def.) patient PBMC before therapy (upper left), after 3months (upper right), 8 months (lower left), and 12 months (lower right). Red dots: fold change ≥ 2; blue dots: fold change ≤ 2. Dashed line: P=0.01; dotted line: P=0.05.
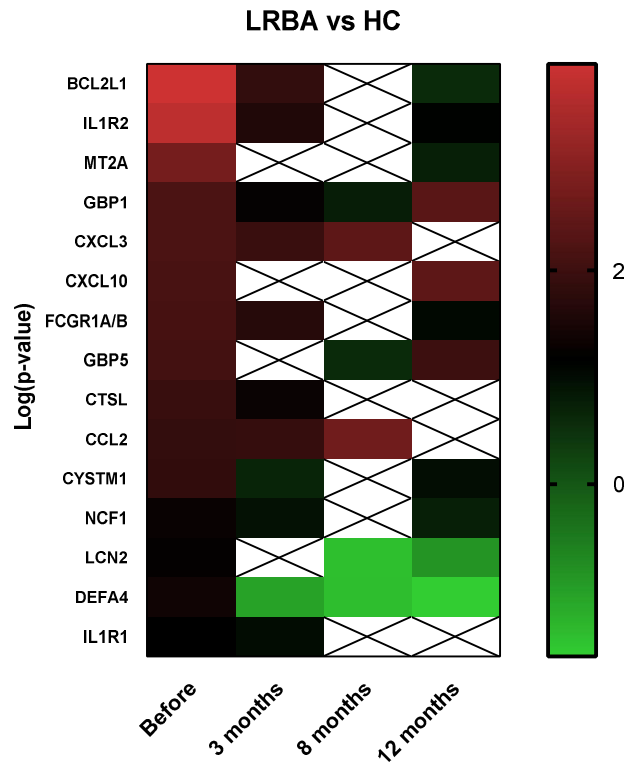
Figure 4.4 Heatmap of differentially expressed genes between healthy and LATAIE patient PBMC before therapy, after 3 months, 8 months, and 12 months using the Host Response gene panel. Fold changes are calculated on the baseline of healthy control. Data points with P<0.05 were excluded. (P: patient; HC: healthy control)

At this point, our gene expression analysis and functional experiments are in ongoing development, but our preliminary results suggest that abatacept therapy in CHAI and LATAIE patients improves the autoinflammatory gene expression profile within 3 months, persisting up to 12 months with continuous treatment. The functions of the LRBA protein in other cellular processes are yet to be clarified, but our gene expression data indicates it could be productive to functionally further explore its involvement in apoptosis and autophagy associated pathways. In accordance with the notion made in previous work by Lo et al. that LRBA is involved in the regulation of cellular recycling vesicles, vital roles in the maintenance of protein homeostasis explaining the variation in severity between CHAI and LATAIE pathophysiology might be revealed.

CHAPTER 5

CONCLUSION

In our laboratory, we have been studying the functional implications of various primary immune deficiencies (PIDs) with a focus on innate immune activation pathways. Herein, our main intention has been to clarify the underlying mechanisms that might have instigated the autoinflammatory pathogenesis in a case of NEMO deficiency. Secondly, we attempted to gain insights into the gene expression profiles in a cohort of CHAI and LATAIE patients with the purpose of finding disease associated indications to further pursue using functional assays.

The 419 amino acid long NEMO (IKK-γ) protein executes multiple fundamental roles involved in cellular homeostasis through its coiled-coil (CC1 and CC2), leucine zipper (LZ), and zinc finger (ZF) motifs. Its importance in innate immunity stems from its regulatory part in the activation of the IKK complex and subsequent NF-κB signaling. Mutations in male that lead to the absence of whole NEMO are embryonically lethal, whereas females develop incontinentia pigmenti (IP). The subject of this study was identified to have aquired a nonsense mutation at p.Gln205* causing the loss of the CC2, LZ, and ZF domains, who later underwent HSCT. Another previously documented patient with the same mutation was shown to abundantly express the shorter isoform of NEMO that is ~40kDa in molecular size, while lacking the 48kDa whole protein. Although we tried to detect either a short truncated protein or an isoform as reported before by approaching with alternative antibodies specific for both the C- and N-terminus, we could not observe any bands, while healthy controls had clearly two bands. We think that any form of NEMO that the patient had been utilizing was subjected to degradation due to the chronic inflammatory state at the time the sample was taken, rendering it undetectable with immunoblotting, which unopportunely remained the limitation of this study.

As expected due to the impairment in NF-κB signal transduction, the patient was unable to secrete the pro-inflammatory cytokines IL-1β and IL-6 following TLR activation. As T-cell activation through the PKC-θ pathway also requires NF-κB signaling, the patient could not secrete IFN-γ after T-cell stimulation with PMA/ionomycin. Nevertheless, the patient exhibited recurrent fever in the clinical course, meaning that the ability to produce acute phase proteins was intact. This indicates that the NEMO protein was able to carry out partial tasks but inefficient to constitute a fully functional immune system.

We conducted two different gene expression analysis, one with the Inflammation panel and the second with the PanCancer Immune Profiling panel. Both analyses converged on the outcome of reduced pro-inflammatory cytokine genes such as *il6* or *il1b* but interestingly had highly elevated levels of inflammatory granulocyte associated genes known as *ltf*, *lcn2*, *ceacam8*, and *ctsg*. LTF, LCN2, and cathepsin G are found in neutrophil granules and while the former two are antimicrobial peptides, the latter is a serine protease also able to act on pathogens. CEACAM8 (CD66b) is a surface adhesion molecule that is found on activated neutrophils. This gene expression data, complemented with the flow cytometric detection of ~35% LDG in the PBMC of the patient suggests a damaging role of circulating LDG in the clinical autoinflammation.

Normal density neutrophils contain the enzyme NADPH-oxidase responsible for the production of ROS at their primed state. Our flow cytometry analysis of the activation status of autologous neutrophils isolated from the patient revealed ROS accumulation in NEMO deficient unstimulated neutrophils compared to healthy neutrophils, indicating their potential contribution to the autoinflammatory pathophysiology observed in the patient. Interestingly, the patient displayed an elevated type I IFN signature as evidenced by high levels of IP-10 in the plasma as well as excessive ISGylation of PBMC proteins and free ISG15 in the patient compared to healthy control. It is possible that a mutant NEMO protein is able to

bind TBK1 (TANK binding kinase 1), a member in the signaling cascade for IFN production, which might be the cause of high type I IFN in the patient.

Collectively, this part of the study shows for the first time an inflammatory population of LDG and primed neutrophils triggered by the presence of spontaneous type I IFN can be the origin of autoinflammatory manifestations in NEMO deficiency, thereby proposing potential novel targets for therapeutic interventions.

In the second part of our study we collected RNA samples isolated from CHAI and LATAIE patient PBMC, who started abatacept therapy and performed gene expression analysis using the Host Response panel on different time points in the course of treatment. Both disorders originate from the diminished presence of CTLA-4 on the cell membrane of activated and regulatory T-cells. CTLA-4 restricts immune activation of T-cells and indirectly B-cells through helper T-cell inhibition by competing with the CD28 receptor on T-cells with superior affinity and avidity for binding to its ligands CD80 and CD86 on APCs. LRBA takes up a protective role for CTLA-4 that is present in recycling endosomes, by binding its cytoplasmic tail dımain and preventing its interaction with the AP-1 adaptor, which upon access targets CTLA-4 for premature lysosomal degradation. Although the severity and age of onset differ in both disorders, patients display symptoms of similar nature such as lymphocytic infiltration of the gut, brain, or lungs as well as autoimmune cytopenia, lymphadenopathy, and hypogammaglobulinemia.

We observed upregulation of gene groups in accordance with the clinical manifestations of the patients before therapy. For instance, genes associated with immune exhaustion like *tigit* and *havcr2* as well as the gene related to for cell-to-matrix *thbs1* interactions were upregulated in CHAI patients, but normalize after abatacept therapy. LATAIE patients, on the other hand, display elevated levels of genes related to apoptosis and autophagy such as *bcl2l1*, encoding for the protein Bcl-x, which depending on the size of the short or long variant, inhibits or supports apoptosis, respectively. Common for both group of patients, gene groups specific to

neutrophil granules like *defa4* or *lcn2* are also downregulated during the course of treatment. Interestingly, chemokine associated genes such as *cxcl3* or *ccl2* remain elevated even after 12 months of treatment. This part of the study is in ongoing expansion, however our data revealed that abatacept therapy alleviates the inflammatory gene expression profile in both groups of patients

REFERENCES

Acuto, O., & Michel, F. (2003). CD28-mediated co-stimulation: a quantitative support for TCR signalling. *Nature Reviews. Immunology, 3*(12), 939–951. https://doi.org/10.1038/NRI1248

Aderem, A., & Underhill, D. M. (2003). MECHANISMS OF PHAGOCYTOSIS IN MACROPHAGES. *Http://Dx.Doi.Org/10.1146/Annurev.Immunol.17.1.593, 17*, 593–623. https://doi.org/10.1146/ANNUREV.IMMUNOL.17.1.593

Adrover, J. M., del Fresno, C., Crainiciuc, G., Cuartero, M. I., Casanova-Acebes, M., Weiss, L. A., … Hidalgo, A. (2019). A Neutrophil Timer Coordinates Immune Defense and Vascular Protection. *Immunity, 51*(5), 966–967. https://doi.org/10.1016/J.IMMUNI.2019.11.001

Arts, R. J. W., Moorlag, S. J. C. F. M., Novakovic, B., Li, Y., Wang, S. Y., Oosting, M., … Netea, M. G. (2018). BCG Vaccination Protects against Experimental Viral Infection in Humans through the Induction of Cytokines Associated with Trained Immunity. *Cell Host and Microbe, 23*(1), 89-100.e5. https://doi.org/10.1016/j.chom.2017.12.010

Baeuerle, P. A., & Baltimore, D. (1988). Activation of DNA-binding activity in an apparently cytoplasmic precursor of the NF-κB transcription factor. *Cell, 53*(2), 211–217. https://doi.org/10.1016/0092-8674(88)90382-0

Bennett, L., Palucka, A. K., Arce, E., Cantrell, V., Borvak, J., Banchereau, J., & Pascual, V. (2003). Interferon and granulopoiesis signatures in systemic lupus erythematosus blood. *Journal of Experimental Medicine, 197*(6), 711–723. https://doi.org/10.1084/jem.20021553

Beutler, B., & Rietschel, E. T. (2003). Innate immune sensing and its roots: the story of endotoxin. *Nature Reviews. Immunology, 3*(2), 169–176.

https://doi.org/10.1038/NRI1004

Bogdan, C., Röllinghoff, M., & Diefenbach, A. (2000). Reactive oxygen and reactive nitrogen intermediates in innate and specific immunity. *Current Opinion in Immunology*, *12*(1), 64–76. https://doi.org/10.1016/S0952-7915(99)00052-7

Borregaard, N., & Cowland, J. B. (1997). Granules of the Human Neutrophilic Polymorphonuclear Leukocyte. *Blood*, *89*(10), 3503–3521. https://doi.org/10.1182/BLOOD.V89.10.3503

Brinkmann, V., & Zychlinsky, A. (2007). Beneficial suicide: why neutrophils die to make NETs. *Nature Reviews. Microbiology*, *5*(8), 577–582. https://doi.org/10.1038/NRMICRO1710

Cai, X., Chiu, Y. H., & Chen, Z. J. (2014). The cGAS-cGAMP-STING pathway of cytosolic DNA sensing and signaling. *Molecular Cell*, *54*(2), 289–296. https://doi.org/10.1016/J.MOLCEL.2014.03.040

Chen, L., & Flies, D. B. (2013). Molecular mechanisms of T cell co-stimulation and co-inhibition. *Nature Reviews. Immunology*, *13*(4), 227–242. https://doi.org/10.1038/NRI3405

Chertov, O., Yang, D., Zack Howard, O. M., & Oppenheim, J. J. (2000). Leukocyte granule proteins mobilize innate host defenses and adaptive immune responses. *Immunological Reviews*, *177*, 68–78. https://doi.org/10.1034/J.1600-065X.2000.17702.X

Dahlgren, C., & Karlsson, A. (1999). Respiratory burst in human neutrophils. *Journal of Immunological Methods*, *232*(1–2), 3–14. https://doi.org/10.1016/S0022-1759(99)00146-5

Denny, M. F., Yalavarthi, S., Zhao, W., Thacker, S. G., Anderson, M., Sandy, A. R., … Kaplan, M. J. (2010). A Distinct Subset of Proinflammatory Neutrophils Isolated from Patients with Systemic Lupus Erythematosus

Induces Vascular Damage and Synthesizes Type I IFNs. *The Journal of Immunology*, *184*(6), 3284–3297. https://doi.org/10.4049/jimmunol.0902199

Frauwirth, K. A., Riley, J. L., Harris, M. H., Parry, R. V., Rathmell, J. C., Plas, D. R., … Thompson, C. B. (2002). The CD28 signaling pathway regulates glucose metabolism. *Immunity*, *16*(6), 769–777. https://doi.org/10.1016/S1074-7613(02)00323-0

Fusco, F., Pescatore, A., Conte, M. I., Mirabelli, P., Paciolla, M., Esposito, E., … Ursini, M. V. (2015). EDA-ID and IP, Two Faces of the Same Coin: How the Same IKBKG / NEMO Mutation Affecting the NF-B Pathway Can Cause Immunodeficiency and/or Inflammation. *International Reviews of Immunology*, *34*(6), 445–459. https://doi.org/10.3109/08830185.2015.1055331

Gámez-Díaz, L., August, D., Stepensky, P., Revel-Vilk, S., Seidel, M. G., Noriko, M., … Grimbacher, B. (2016). The extended phenotype of LPS-responsive beige-like anchor protein (LRBA) deficiency. *The Journal of Allergy and Clinical Immunology*, *137*(1), 223–230. https://doi.org/10.1016/J.JACI.2015.09.025

Gudmundsdottir, H., Wells, A. D., & Turka, L. A. (1999). Dynamics and requirements of T cell clonal expansion in vivo at the single-cell level: effector function is linked to proliferative capacity. *Journal of Immunology (Baltimore, Md. : 1950)*, *162*(9), 5212–5223. Retrieved from http://www.ncbi.nlm.nih.gov/pubmed/10227995

Gul, E., Sayar, E. H., Gungor, B., Eroglu, F. K., Surucu, N., Keles, S., … Gursel, M. (2018). Type I IFN–related NETosis in ataxia telangiectasia and Artemis deficiency. *Journal of Allergy and Clinical Immunology*, *142*(1), 246–257. https://doi.org/10.1016/j.jaci.2017.10.030

Hacbarth, E., & Kajdacsy☐Balla, A. (1986). Low density neutrophils in patients with systemic lupus erythematosus, rheumatoid arthritis, and acute rheumatic

fever. *Arthritis & Rheumatism*, *29*(11), 1334–1342.
https://doi.org/10.1002/art.1780291105

Häcker, H., & Karin, M. (2006). Regulation and function of IKK and IKK-related
kinases. *Science's STKE : Signal Transduction Knowledge Environment*,
2006(357). https://doi.org/10.1126/stke.3572006re13

Hayden, M. S., & Ghosh, S. (2008). Shared Principles in NF-κB Signaling. *Cell*,
132(3), 344–362. https://doi.org/10.1016/J.CELL.2008.01.020

Heil, F., Hemmi, H., Hochrein, H., Ampenberger, F., Kirschning, C., Akira, S., …
Bauer, S. (2004). Species-specific recognition of single-stranded RNA via
toll-like receptor 7 and 8. *Science (New York, N.Y.)*, *303*(5663), 1526–1529.
https://doi.org/10.1126/SCIENCE.1093620

Hidalgo, A., Chilvers, E. R., Summers, C., & Koenderman, L. (2019). The
Neutrophil Life Cycle. *Trends in Immunology*, *40*(7), 584–597.
https://doi.org/10.1016/j.it.2019.04.013

Hodi, F. S., O'Day, S. J., McDermott, D. F., Weber, R. W., Sosman, J. A., Haanen,
J. B., … Urba, W. J. (2010). Improved survival with ipilimumab in patients
with metastatic melanoma. *The New England Journal of Medicine*, *363*(8),
711–723. https://doi.org/10.1056/NEJMOA1003466

Honda, K., Takaoka, A., & Taniguchi, T. (2006). Type I interferon [corrected] gene
induction by the interferon regulatory factor family of transcription factors.
Immunity, *25*(3), 349–360. https://doi.org/10.1016/J.IMMUNI.2006.08.009

Honda, K., & Taniguchi, T. (2006). IRFs: master regulators of signalling by Toll-
like receptors and cytosolic pattern-recognition receptors. *Nature Reviews.
Immunology*, *6*(9), 644–658. https://doi.org/10.1038/NRI1900

Hornung, V., Ablasser, A., Charrel-Dennis, M., Bauernfeind, F., Horvath, G.,
Caffrey, D. R., … Fitzgerald, K. A. (2009). AIM2 recognizes cytosolic
dsDNA and forms a caspase-1-activating inflammasome with ASC. *Nature*,

76

458(7237), 514–518. https://doi.org/10.1038/NATURE07725

Hornung, V., Ellegast, J., Kim, S., Brzózka, K., Jung, A., Kato, H., … Hartmann, G. (2006). 5'-Triphosphate RNA is the ligand for RIG-I. *Science (New York, N.Y.)*, *314*(5801), 994–997. https://doi.org/10.1126/SCIENCE.1132505

Hsia, C. Y., Cheng, S., Owyang, A. M., Dowdy, S. F., & Liou, H. C. (2002). c-Rel regulation of the cell cycle in primary mouse B lymphocytes. *International Immunology*, *14*(8), 905–916. https://doi.org/10.1093/INTIMM/DXF055

Ishikawa, H., & Barber, G. N. (2008). STING is an endoplasmic reticulum adaptor that facilitates innate immune signalling. *Nature*, *455*(7213), 674–678. https://doi.org/10.1038/NATURE07317

Janeway, C. A., & Medzhitov, R. (2003). Innate Immune Recognition. *Https://Doi.Org/10.1146/Annurev.Immunol.20.083001.084359*, *20*, 197–216. https://doi.org/10.1146/ANNUREV.IMMUNOL.20.083001.084359

Jin, M. S., Kim, S. E., Heo, J. Y., Lee, M. E., Kim, H. M., Paik, S. G., … Lee, J. O. (2007). Crystal structure of the TLR1-TLR2 heterodimer induced by binding of a tri-acylated lipopeptide. *Cell*, *130*(6), 1071–1082. https://doi.org/10.1016/J.CELL.2007.09.008

Karin, M., & Delhase, M. (2000). The IκB kinase (IKK) and NF-κB: Key elements of proinflammatory signalling. *Seminars in Immunology*, *12*(1), 85–98. https://doi.org/10.1006/smim.2000.0210

Karin, Michael. (1999). How NF-κB is activated: the role of the IκB kinase (IKK) complex. *Oncogene 1999 18:49*, *18*(49), 6867–6874. https://doi.org/10.1038/sj.onc.1203219

Kato, H., Takeuchi, O., Sato, S., Yoneyama, M., Yamamoto, M., Matsui, K., … Akira, S. (2006). Differential roles of MDA5 and RIG-I helicases in the recognition of RNA viruses. *Nature*, *441*(7089), 101–105. https://doi.org/10.1038/NATURE04734

Kawai, T., & Akira, S. (2007). Signaling to NF-κB by Toll-like receptors. *Trends in Molecular Medicine*, *13*(11), 460–469. https://doi.org/10.1016/J.MOLMED.2007.09.002

Kawai, T., Sato, S., Ishii, K. J., Coban, C., Hemmi, H., Yamamoto, M., … Akira, S. (2004). Interferon-alpha induction through Toll-like receptors involves a direct interaction of IRF7 with MyD88 and TRAF6. *Nature Immunology*, *5*(10), 1061–1068. https://doi.org/10.1038/NI1118

Klemann, C., Pannicke, U., Morris-Rosendahl, D. J., Vlantis, K., Rizzi, M., Uhlig, H., … Rohr, J. C. (2016). Transplantation from a symptomatic carrier sister restores host defenses but does not prevent colitis in NEMO deficiency. *Clinical Immunology*, *164*, 52–56. https://doi.org/10.1016/j.clim.2016.01.010

Kofoed, E. M., & Vance, R. E. (2011). Innate immune recognition of bacterial ligands by NAIPs determines inflammasome specificity. *Nature*, *477*(7366), 592–597. https://doi.org/10.1038/NATURE10394

Kolaczkowska, E., & Kubes, P. (2013). Neutrophil recruitment and function in health and inflammation. *Nature Reviews. Immunology*, *13*(3), 159–175. https://doi.org/10.1038/NRI3399

Kruzel, M. L., Zimecki, M., & Actor, J. K. (2017). Lactoferrin in a context of inflammation-induced pathology. *Frontiers in Immunology*. https://doi.org/10.3389/fimmu.2017.01438

Levy, D. E., & Darnell, J. E. (2002). Stats: transcriptional control and biological impact. *Nature Reviews. Molecular Cell Biology*, *3*(9), 651–662. https://doi.org/10.1038/NRM909

Liu, A. R., & Ramakrishnan, P. (2021). Regulation of Nuclear Factor-kappaB Function by O-GlcNAcylation in Inflammation and Cancer. *Frontiers in Cell and Developmental Biology*, *9*, 2894. https://doi.org/10.3389/FCELL.2021.751761/BIBTEX

Liu, L., Botos, I., Wang, Y., Leonard, J. N., Shiloach, J., Segal, D. M., & Davies, D. R. (2008). Structural basis of toll-like receptor 3 signaling with double-stranded RNA. *Science (New York, N.Y.)*, *320*(5874), 379–381. https://doi.org/10.1126/SCIENCE.1155406

Liu, M., Guo, S., Hibbert, J. M., Jain, V., Singh, N., Wilson, N. O., & Stiles, J. K. (2011). CXCL10/IP-10 in infectious diseases pathogenesis and potential therapeutic implications. *Cytokine and Growth Factor Reviews*, *22*(3), 121–130. https://doi.org/10.1016/j.cytogfr.2011.06.001

Liu, S., Cai, X., Wu, J., Cong, Q., Chen, X., Li, T., … Chen, Z. J. (2015). Phosphorylation of innate immune adaptor proteins MAVS, STING, and TRIF induces IRF3 activation. *Science (New York, N.Y.)*, *347*(6227). https://doi.org/10.1126/SCIENCE.AAA2630

Lo, B., Fritz, J. M., Su, H. C., Uzel, G., Jordan, M. B., & Lenardo, M. J. (2016). CHAI and LATAIE: new genetic diseases of CTLA-4 checkpoint insufficiency. *Blood*, *128*(8), 1037–1042. https://doi.org/10.1182/BLOOD-2016-04-712612

Lo, B., Zhang, K., Lu, W., Zheng, L., Zhang, Q., Kanellopoulou, C., … Jordan, M. B. (2015). Patients with LRBA deficiency show CTLA4 loss and immune dysregulation responsive to abatacept therapy. *Science*, *349*(6246), 436–440. https://doi.org/10.1126/science.aaa1663

Loeb, K. R., & Haas, A. L. (1992). The interferon-inducible 15-kDa ubiquitin homolog conjugates to intracellular proteins. *Journal of Biological Chemistry*, *267*(11), 7806–7813. https://doi.org/10.1016/s0021-9258(18)42585-9

Lund, J., Sato, A., Akira, S., Medzhitov, R., & Iwasaki, A. (2003). Toll-like receptor 9-mediated recognition of Herpes simplex virus-2 by plasmacytoid dendritic cells. *The Journal of Experimental Medicine*, *198*(3), 513–520. https://doi.org/10.1084/JEM.20030162

Malterer, M. B., Glass, S. J., & Newman, J. P. (2014). Interferon-stimulated genes:

A complex web of host defenses. *Annual Review of Immunology*, *44*(3), 735–745. https://doi.org/10.1038/jid.2014.371

Mayadas, T. N., Cullere, X., & Lowell, C. A. (2014). The multifaceted functions of neutrophils. *Annual Review of Pathology*, *9*, 181–218. https://doi.org/10.1146/ANNUREV-PATHOL-020712-164023

Murphy, K. M., & Reiner, S. L. (2002). The lineage decisions of helper T cells. *Nature Reviews. Immunology*, *2*(12), 933–944. https://doi.org/10.1038/NRI954

Notarangelo, L. D., Bacchetta, R., Casanova, J. L., & Su, H. C. (2020). Human inborn errors of immunity: An expanding universe. *Science Immunology*, *5*(49). https://doi.org/10.1126/sciimmunol.abb1662

Park, B. S., Song, D. H., Kim, H. M., Choi, B. S., Lee, H., & Lee, J. O. (2009). The structural basis of lipopolysaccharide recognition by the TLR4-MD-2 complex. *Nature*, *458*(7242), 1191–1195. https://doi.org/10.1038/NATURE07830

Perng, Y. C., & Lenschow, D. J. (2018). ISG15 in antiviral immunity and beyond. *Nature Reviews Microbiology*, *16*(7), 423–439. https://doi.org/10.1038/s41579-018-0020-5

Pichlmair, A., Schulz, O., Tan, C. P., Näslund, T. I., Liljeström, P., Weber, F., & Reis E Sousa, C. (2006). RIG-I-mediated antiviral responses to single-stranded RNA bearing 5'-phosphates. *Science (New York, N.Y.)*, *314*(5801), 997–1001. https://doi.org/10.1126/SCIENCE.1132998

Pott, J., Mahlakõiv, T., Mordstein, M., Duerr, C. U., Michiels, T., Stockinger, S., … Hornef, M. W. (2011). IFN-lambda determines the intestinal epithelial antiviral host defense. *Proceedings of the National Academy of Sciences of the United States of America*, *108*(19), 7944–7949. https://doi.org/10.1073/PNAS.1100552108

Ramírez-Alejo, N., Alcántara-Montiel, J. C., Yamazaki-Nakashimada, M., Duran-McKinster, C., Valenzuela-León, P., Rivas-Larrauri, F., … Santos-Argumedo, L. (2015). Novel hypomorphic mutation in IKBKG impairs NEMO-ubiquitylation causing ectodermal dysplasia, immunodeficiency, incontinentia pigmenti, and immune thrombocytopenic purpura. *Clinical Immunology*, *160*(2), 163–171. https://doi.org/10.1016/j.clim.2015.06.007

Rosales, C. (2018). Neutrophil: A cell with many roles in inflammation or several cell types? *Frontiers in Physiology*, *9*(FEB), 1–17. https://doi.org/10.3389/fphys.2018.00113

Rudd, C. E., Taylor, A., & Schneider, H. (2009). CD28 and CTLA-4 coreceptor expression and signal transduction. *Immunological Reviews*, *229*(1), 12–26. https://doi.org/10.1111/J.1600-065X.2009.00770.X

Sharpe, A. H. (2009). Mechanisms of Costimulation. *Immunological Reviews*, *229*(1), 5. https://doi.org/10.1111/J.1600-065X.2009.00784.X

Shaw, M. H., Reimer, T., Kim, Y. G., & Nuñez, G. (2008). NOD-like receptors (NLRs): bona fide intracellular microbial sensors. *Current Opinion in Immunology*, *20*(4), 377–382. https://doi.org/10.1016/J.COI.2008.06.001

Smahl, A., Courtols, G., Vabres, P., Yamaoka, S., Heuertz, S., Munnich, A., … Nelson, D. L. (2000). Genomic rearrangement in NEMO impairs NF-κB activation and is a cause of incontinentia pigmenti. *Nature*, *405*(6785), 466–472. https://doi.org/10.1038/35013114

Strober, W., Murray, P. J., Kitani, A., & Watanabe, T. (2006). Signalling pathways and molecular interactions of NOD1 and NOD2. *Nature Reviews. Immunology*, *6*(1), 9–20. https://doi.org/10.1038/NRI1747

Sun, S. C., & Ley, S. C. (2008). New insights into NF-κB regulation and function. *Trends in Immunology*, *29*(10), 469. https://doi.org/10.1016/J.IT.2008.07.003

Tanaka, Y., & Chen, Z. J. (2012). STING specifies IRF3 phosphorylation by TBK1

in the cytosolic DNA signaling pathway. *Science Signaling*, *5*(214), 1–12. https://doi.org/10.1126/scisignal.2002521

Wang, J.-W., Howson, J., Haller, E., & Kerr, W. G. (2001). Identification of a novel lipopolysaccharide-inducible gene with key features of both A kinase anchor proteins and chs1/beige proteins. *Journal of Immunology (Baltimore, Md. : 1950)*, *166*(7), 4586–4595. https://doi.org/10.4049/JIMMUNOL.166.7.4586

Werts, C., Girardin, S. E., & Philpott, D. J. (2006). TIR, CARD and PYRIN: three domains for an antimicrobial triad. *Cell Death and Differentiation*, *13*(5), 798–815. https://doi.org/10.1038/SJ.CDD.4401890

APPENDICES

A. Culture Media, Buffers and Solutions

<u>RPMI-1640 (Gibco) supplemented with L-Glutamine</u>

2 % :10 ml FBS (FBS is inactivated at 55°C)

5 %: 5 ml FBS

10 %: 50 ml FBS

5 ml Penicillin/Streptomycin (50µg/ml final concentration from 10 mg/ml stock)

5 ml HEPES (Biological Industries), (10mM final concentration from 1 M stock)

5 ml Na Pyruvate, (0,11 mg/ml final concentration from 100mM, 11 mg/ml stock)

5 ml Non-Essential Amino Acids Solution, (diluted into 1x from 100x concentrate stock)

<u>BS-BSA-Na azide (FACS Buffer)</u>

500 ml 1x PBS

5g BSA (1%)

125mg (0,25%)

<u>Blocking Buffer (ELISA)</u>

500ml 1x PBS

25 grams BSA (5%)

250µl Tween20 (0,025%)

Crystal particles of BSA should be dissolved very well, with magnetic-heating stirrer for 20-30 min. The buffer should be stored at -20°C.

Wash Buffer [ELISA]

500 ml 10x PBS

2,5 ml Tween20

4,5lt ddH2O

Running Buffer (10x)

SDS-PAGE 10× SDS Running Buffer

Tris base 30.3 g

Glycine 144.4 g

SDS 10 g

Dissolve in 1 L of -filtered H2O and reduce to 1x concentration before use

Transfer Buffer (1x).

Transfer buffer for western blotting

25 mM Tris-HCl (pH 7.6)

192 mM glycine

20% methanol

0.03% sodium dodecyl sulfate (SDS)

Tris Buffered Saline (TBS)

NaCl 8 g

KCl 0.2 g

Tris base 3 g

Phenol red 0.015 g

Add 0.1% Tween20 before use

CURRICULUM VITAE

PERSONAL INFORMATION

Surname, Name: Sürücü, Naz
Nationality: Turkish (TC)
Date and Place of Birth: 2 January 1990, Altındağ
Marital Status: Single
Phone: +90 539 212 7539
Email: nazsrc@gmail.com

EDUCATION

Degree	Institution	Year of Graduation
MS	METU Biological Sciences	2017
BS	METU Biological Sciences	2015
High School	Atatürk Anadolu High School, Ankara	2009

WORK EXPERIENCE

Year	Place	Enrollment
2015-Present	Immunology laboratory of Prof. Mayda Gursel	MS and PhD student

FOREIGN LANGUAGES

Advanced English and German

PUBLICATIONS

1. Gul, E., Sayar, E. H., Gungor, B., Eroglu, F. K., Surucu, N., Keles, S., Guner, S. N., Findik, S., Alpdundar, E., Ayanoglu, I. C., Kayaoglu, B., Geckin, B. N., Sanli, H. A., Kahraman, T., Yakicier, C., Muftuoglu, M., Oguz, B., Cagdas Ayvaz, D. N., Gursel, I., Ozen, S., Reisli, I., & Gursel, M. (2018). Type I IFN–related NETosis in ataxia telangiectasia and Artemis deficiency. J. Allergy Clin. Immunol., 142(1), 246–257

2. Çağdaş, D., Sürücü, N., Tan, Ç., Kayaoğlu, B., Özgül, R. K., Akkaya-Ulum, Y. Z., Aydınoğlu, A. T., Aytaç, S., Gümrük, F., Balci-Hayta, B., Balci-

Peynircioğlu, B., Özen, S., Gürsel, M., & Tezcan, İ. (2020). Autoinflammation in addition to combined immunodeficiency: SLC29A3 gene defect. Mol. Immunol., 121, 28–37.

3. Alpdundar Bulut, E., Bayyurt Kocabas, B., Yazar, V., Aykut, G., Guler, U., Salih, B., Surucu Yilmaz, N., Ayanoglu, I. C., Polat, M. M., Akcali, K. C., Gursel, I., & Gursel, M. (2020). Human Gut Commensal Membrane Vesicles Modulate Inflammation by Generating M2-like Macrophages and Myeloid-Derived Suppressor Cells. J. Immunol., 205(10), 2707–2718.

4. Kayaoglu, B., Kasap, N., Yilmaz, N. S., Charbonnier, L. M., Geckin, B., Akcay, A., Eltan, S. B., Ozturk, G., Ozen, A., Karakoc-Aydiner, E., Chatila, T. A., Gursel, M., & Baris, S. (2021). Stepwise Reversal of Immune Dysregulation Due to STAT1 Gain-of-Function Mutation Following Ruxolitinib Bridge Therapy and Transplantation. J. Clin. Immunol.

5. Yilmaz, IC; Ipekoglu, EM; Bulbul, A; Turay, N; Yildirim, M; Evcili, I; Surucu Yilmaz, Naz; Guvencli, N; Aydin, Y; Gungor, B; Saraydar, B; Bartan, AG; Ibibik, B; Bildik, T; Baydemir, I; Sanli, HA; Kayaoglu, B; Ceylan, Y; Yildirim, T; Abras, I; Ayanoglu, IC; Cam, SB; Ciftci Dede, E; Gizer, M; Erganis, O; Sarac, F; Uzar, S; Enul, H; Adiay, C; Aykut, G; Polat, H; Yildirim, IS; Tekin, S; Korukluoglu, G; Zeytin, HE; Korkusuz, P; Gursel, I; Gursel, M. (2021) Development and preclinical evaluation of virus-like particle vaccine against COVID-19 infection. Allergy.

6. Yilmaz, NS; Eltan SB; Kayaoglu B; Geckin B; Heredia RJ; Sefer AP; Kiykim A; Nain E; Kasap N; Dogru O; Yucelten AD; Cinel L; Karasu G; Yesilipek A; Sozeri B; Kaya GG; Yilmaz IC; Baydemir I; Aydin Y; Kahraman DC; Haimel M; Boztug K; Aydiner EK; Gursel I; Ozen A; Baris S; Gursel M. (2022), Low Density Granulocytes and Dysregulated Neutrophils Driving Autoinflammatory Manifestations in NEMO Deficiency *Journal of Clinical Immunology*.

7. Asena Pinar Sefer, Hassan Abolhassani, Franziska Ober, Basak Kayaoglu, Sevgi Bilgic Eltan, Altan Kara, Baran Erman, Naz Surucu Yilmaz, Cigdem Aydogmus, Sezin Aydemir, Louis-Marie Charbonnier, Burcu Kolukisa, Gholamreza Azizi, Samaneh Delavari, Tooba Momen, Simuzar Aliyeva, Yasemin Kendir Demirkol, Saban Tekin, Ayca Kiykim, Omer Faruk Baser, Haluk Cokugras, Mayda Gursel, Elif Karakoc-Aydiner, Ahmet Ozen, Daniel Krappmann, Talal A. Chatila, Nima Rezaei & Safa Baris (2022), Expanding the Clinical and Immunological Phenotypes and Natural History of MALT1 Deficiency Journal of Clinical Immunology.